Physica Medica 125 (2024) 103434

Contents lists available at ScienceDirect

Physica Medica

journal homepage: www.elsevier.com/locate/ejmp

Review paper

An inventory of patient-image based risk/dose, image quality and body habitus/size metrics for adult abdomino-pelvic CT protocol optimisation

Eric Pace [a,*], Carmel J. Caruana [a], Hilde Bosmans [b], Kelvin Cortis [c], Melvin D'Anastasi [c], Gianluca Valentino [d]

[a] Medical Physics, Faculty of Health Science, University of Malta, Msida MSD2080, Malta
[b] Medical Physics & Quality Assessment, Department of Imaging & Pathology, KU Leuven, Leuven, Belgium
[c] Medical Imaging Department, Mater Dei Hospital, Msida MSD2090, Malta
[d] Communications & Computer Engineering Department, Faculty of Information and Communication Technology, University of Malta, Msida MSD2080, Malta

ARTICLE INFO

Keywords:
Abdomino-pelvic
Comput* tomography
Protocol optimization
Image quality
Body habitus/size
Patient dose/risk

ABSTRACT

Purpose: Patient-specific protocol optimisation in abdomino-pelvic Computed Tomography (CT) requires measurement of body habitus/size (BH), sensitivity–specificity (surrogates image quality (IQ) metrics) and risk (surrogates often dose quantities) (RD). This work provides an updated inventory of metrics available for each of these three categories of optimisation variables derivable directly from patient measurements or images. We consider objective IQ metrics mostly in the spatial domain (i.e., those related directly to sharpness, contrast, noise quantity/texture and perceived detectability as these are used by radiologists to assess the acceptability or otherwise of patient images in practice).
Materials and methods: The search engine used was PubMed with the search period being 2010–2024. The key words used were: 'comput* tomography', 'CT', 'abdom*', 'dose', 'risk', 'SSDE', 'image quality', 'water equivalent diameter', 'size', 'body composition', 'habit*', 'BMI', 'obes*', 'overweight'. Since BH is critical for patient specific optimisation, articles correlating RD vs BH, and IQ vs BH were reviewed.
Results: The inventory includes 11 BH, 12 IQ and 6 RD metrics. 25 RD vs BH correlation studies and 9 IQ vs BH correlation studies were identified. 7 articles in the latter group correlated metrics from all three categories concurrently.
Conclusions: Protocol optimisation should be fine-tuned to the level of the individual patient and particular clinical query. This would require a judicious choice of metrics from each of the three categories. It is suggested that, for increased utility in clinical practice, more future optimisation studies be clinical task based and involve the three categories of metrics concurrently.

1. Introduction

Computed Tomography (CT) is well established as a reliable, fast and effective modality for diagnostic imaging, and its use has grown exponentially since its clinical debut in the 1970s [1,2], notwithstanding the advent of MRI. In particular, for acute non-localised abdomino-pelvic pain, the ACR Appropriateness Criteria® advise that a CT abdomino-pelvic scan both with and possibly without intra-venous (IV) contrast would or may be appropriate, making CT an essential modality for the emergency department [3].

Although patient doses for typical abdominal and abdomino-pelvic imaging have decreased over time [4,5], techniques such as multi-phasic CT and volumetric imaging have resulted in an increase in the collective dose, particularly for some patient groups [4–6] and in particular larger patients [7–12]. Optimisation of abdomino-pelvic CT protocols is therefore an ongoing concern.

Protocol optimisation in abdomino-pelvic CT hinges on the use of accurate estimates of body habitus/size (BH) metrics, sensitivity–specificity metrics relevant to the particular clinical query (surrogates being quantitative, ideally objective, image quality (IQ) metrics relevant to the specific clinical query) and patient risk metrics (surrogates often patient risk/dose (RD) metrics). Protocol optimisation should ideally be fine-

* Corresponding author.
E-mail address: eric.pace.08@um.edu.mt (E. Pace).

https://doi.org/10.1016/j.ejmp.2024.103434
Received 3 October 2023; Received in revised form 4 July 2024; Accepted 17 July 2024
Available online 2 August 2024

tuned to the level of the individual patient, or categories of patients, and particular clinical query. This would require a judicious choice of metrics from each of these three categories.

The objective of this literature review was to provide an updated inventory of metrics available for each of these categories and of the available knowledge about the metrics: their definitions, methods used for measurement or calculation and their utility in practice together with their respective strengths and limitations. BH metrics are discussed first: this is because any pre-scanning estimates of image quality and risk/dose metrics need to be based on BH. Metrics for IQ are then discussed, as any discussion on RD metrics would be meaningless without first considering the diagnostic quality of the images. Finally, RD-related metrics are presented.

The three categories of metrics are often surveyed separately. However, in the process of optimisation the three categories are interrelated and this article is perhaps the first attempt to bring them together in a more comprehensive manner. Hence, this work also reports on studies which have investigated the presence of correlations between RD and BH metrics and IQ and BH metrics.

2. Method

The search engine used was PubMed. The articles chosen for establishing the *inventory* were retrieved using the query: ((“comput*”[Title] AND “tomography”[Title]) OR “ct”[Title]) AND “abdom*”[Title] AND (“dose*”[Title] OR “risk”[Title] OR “SSDE”[Title] OR “image quality”[Title] OR “water equivalent diameter”[Title] OR “diameter”[Title] OR “size”[Title] OR “body”[Title] OR “BMI”[Title] OR “habit*”[Title] OR “obes*”[Title] OR “overweight”[Title]) AND ((humans[Filter]) AND (2010:2024[pdat])). Articles involving any of ‘photon-CT’, ‘angiography’, ‘CBCT’, ‘dental’, and ‘micro-CT’ were excluded. The search period was between 2010 and 2024. Articles cited by the chosen articles which included relevant metrics were also included even when published prior to the search period. The total number of articles after applying both inclusion and exclusion criteria was 439.

In terms of the inclusion criteria *for the metrics in the inventory*, we focused on metrics which are accessible to the clinical medical physicist in regular clinics (as opposed to, say, reference centres) and which in principle can be automated for both RD and IQ. In terms of IQ, we made a clear distinction between *image quality metrics reflecting directly the sharpness, contrast, noise magnitude/texture and perceived detectability of patient images* and image quality related *device performance metrics* derived either from images of test objects or estimated from patient image features. Device performance metrics are important in particular for device performance monitoring and inter-device comparisons. However, this article focuses on the category of metrics which are perceived to be more directly related to clinical tasks as these are the qualities that clinicians use to evaluate the quality of the images in routine practice. Such metrics are in the spatial domain. Nevertheless, given the historically extensive and present ongoing use of frequency domain metrics, task-based Modulation Transfer Function (MTF), Noise Power Spectrum (NPS) and detectability are also included. The criteria for inclusion of BH metrics were that the metrics would be related to the abdomino-pelvic region and should be potentially useful as predictors of RD or IQ prior to the patient being scanned or at most following the localiser radiograph. Inclusion criteria for the three categories of metrics are given in Table 1.

In this study we focused on the potential utility of BH metrics for the process of patient specific protocol optimization and pre-scan choice of protocol. It was therefore considered imperative to discuss studies that have attempted to measure the correlation of the various BH metrics to IQ metrics, and others which measured correlation of BH metrics to RD metrics (and including of course any which included all three categories of metrics in a single study). The relevance and importance of each BH metric needs to be understood in terms of its suitability for a particular clinical task as well as its level of correlation (and hence predictive power) with relevant metrics from the other two categories. For example, Body Mass Index (BMI) might be a good indicator of overall patient obesity, but may be less correlated with patient dose metrics for abdomino-pelvic CT than effective diameter, D_E. IQ vs RD metric correlation studies which did not involve BH metrics were excluded from the scope of this study [13–15].

In order to ensure that all articles involving the above two pairs of correlations were identified, the earlier PubMed query was focused to refine the results obtained. For RD v BH metrics, the query used was: ((“comput*”[Title] AND “tomograph*”[Title]) OR “ct”[Title]) AND “abdom*”[Title] AND (“dose*”[Title] OR “risk”[Title] OR “SSDE”[Title]) AND (“water*equivalent diameter”[Title] OR “diameter”[Title] OR “size”[Title] OR “body”[Title] OR “BMI”[Title] OR “habit*”[Title] OR “obes*”[Title] OR “overweight”[Title]) AND ((humans[Filter]) AND (2010:2024[pdat])). The number of retrieved articles was 42, from which articles concerning either paediatric patients, or non-radiation

Table 1
Criteria for including body habitus, image quality and dose metrics in the inventory.

Criterion	Rationale
Body Habitus (BH) metrics	
1. Within or related to the adult abdomino-pelvic region.	This is dictated by the scope of the study.
2. Would possibly act as a predictor of dose or image quality metrics.	Ensures relevance to optimisation work.
3. Can be determined pre-scan or post localiser radiograph.	Required for making pre-exposure patient habitus specific optimisation possible.
Image Quality (IQ) metrics	
1. Objective metrics related to image quality as evaluated by the radiologist in patient images (i.e. sharpness, contrast, noise quantity/texture, perceived detectability), as opposed to device performance.	This qualifies the term ‘image quality metric’ as used in this study.
2. Can be calculated solely from ‘for presentation’ image data.	All such data is available to the clinical medical physicist. On the other hand, this excludes metrics which, for example, require access to scanner raw data and which would require clinical-manufacturer agreements which are often only available to major reference centres.
3. Can be automated in principle and be available immediately post-scan.	To avoid the need for reader time and to be useful in objectively assessing whether a patient needs to be rescanned owing to insufficient image quality.
4. Adult and patient specific.	Required by the increased emphasis on personalised medicine.
Risk/Dose (RD) metrics	
1. Can be calculated solely from DICOM header and image data.	All such data is available to the clinical medical physicist.
2. Can be automated in principle.	To avoid the need for human input and for ongoing dose monitoring.
3. Adult and patient specific.	In an era of personalised medicine and increased awareness of individual radiosensitivity, dose optimisation needs to be patient specific.

Table 2
Patient habitus/size metrics for abdomino-pelvic CT optimisation.

Patient body metric and symbol	Definition, units and anatomical location	Measure/estimate of what?	Measurement method and instant	Use
Patient weight	Patient mass (kg). Global whole body metric.	General indicator of patient size.	Patient scales. Pre-scan or post scan.	Although still used in some studies, it has been largely replaced by other metrics.
Waist circumference (WC), also known as girth.	Measure of patient circumference (in cm). Regional metric measured typically at the umbilical level [16] or midway between the iliac crest and lowest rib [17].	Measure of abdominal obesity.	i. Pre-scan (direct measure using tape measure) ii. Post-scan (manual or automatic contour tracing and measurement)	Pre-scan measurement is fast but rarely done in practice as it reduces patient throughput and depends on cooperation from others. Post-scan measurement depends on contouring accuracy but can be done independently of others.
Waist circumference (WC) to hip circumference (HC) ratio (WHR) [16,18–20].	$WHR = WC/HC$Regional metric measured typically at the waist (see WC) and hip.	Measure of abdominal obesity. WHO defines abdominal obesity in men and women as WHR>0.90 and >0.85, respectively. A WHR>1.0 for either sex is associated with a higher probability of health issues [21].	i. Pre-scan, (direct measure with tape measure) iii. Post-scan (manual or automatic contour tracing and measurement).	Pre-scan measurement is fast but rarely done in practice as it reduces patient throughput and depends on cooperation from others. Post-scan measurement depends on contouring accuracy but can be done independently of others.
Sagittal and lateral diameters (AP, LAT).	Distance from front to back and left to right of the patient (mm). Regional metric measured typically at a central slice within the scanned volume [22].	Thickness and width of patient.	Measured on image post-scout or post-scan images using system callipers. Several approaches are possible (see Fig. 1). The authors suggest the bounding box method for consistency.	May be used as a fast measure of patient size.
Patient cross-sectional area (A).	Area of cross-section of patient. Regional metric measured typically at the level of the umbilicus.		Approximate estimate pre-scan from waist circumference. More accurately post-scan. Number of pixels enclosed by the patient perimeter (set as an ROI) multiplied by the square of the pixel pitch. The pixel pitch is obtained from DICOM Pixel Spacing tag (0028,0030).	May be used as a fast measure of patient size.
Area of circumscribing ellipse (A_{cir}).	Area of an ellipse bounded by the patient bounding box (the cross-section of the patient is modelled as an ellipse). Regional metric measured typically at the level of the umbilicus.	Approximates the patient cross-sectional area	$A = \frac{1}{4}\pi AP{\cdot}LAT(mm^2)$. Measured post-scout or post-scan.	May be used as a fast measure of patient size.
Effective diameter (D_E) [23].	Diameter (mm) of a circle having an area equal to the area of the circumscribing ellipse. Regional metric measured typically at the centre of the body region being scanned [23].		$D_E = \sqrt{AP \times LAT}$. Measured post-scout, or post-scan.	May be used as a fast measure of patient size.
Ellipticity ratio (r) [24].	Ratio of LAT to AP diameters of the circumscribing ellipse. Regional metric measured as the average over the entire scanned volume [24].	The ellipticity ratio provides an easy to calculate patient reference that may be useful to understand the system's angular tube current modulation.	$r = \frac{LAT}{AP}$. Measured post-scout, or post-scan.	May be used as a fast measure of patient cross-sectional shape, that may be useful for understanding the angular tube current modulation.
Water equivalent diameter (D_w) [25].	D_w (mm) diameter of water disc having the same total attenuation coefficient as a patient slice. Averaged regional metric when averaged over the scanned volume.	Diameter is not simply geometrical but includes embedded information about patient attenuation and hence patient dose.	$D_w = 2\sqrt{\left[\frac{1}{1000}\overline{CT(x,y)_{ROI}} + 1\right]\frac{A_{ROI}}{\pi}}$, where $\overline{CT(x,y)_{ROI}}$ is the mean of the linear attenuation values of the pixels in the patient slice and A_{ROI} is the cross-sectional area of the patient as measured in the CT slice. Post-scout, post-scan (latter more reliable).	Used in conjunction with CTDIvol to calculate the size-specific-dose-estimate, SSDE(z) [25].
Body Mass Index (BMI).	$BMI(kg/m^2) = \frac{weight}{height^2}$, Global whole body metric.		Pre-scan, direct measurement with stadiometer for the height and personal digital scales for mass.	Measure of patient obesity. This metric depends on weight and height, which may not always be measured at the time of imaging [26]. BMI does not take into account tissue composition and distribution, which is a function of sex and age [21,27].

(*continued on next page*)

Table 2 (*continued*)

Patient body metric and symbol	Definition, units and anatomical location	Measure/estimate of what?	Measurement method and instant	Use
T-shirt size [2].	XXS to XXL Global whole body metric.	General indicator of patient size and/or degree of obesity.	Pre-scan.	Seven 'T-shirt sizes' are defined separately for different body regions. For the waist the ranges have been defined ranging from XXS (D_E<19 cm), to XXL (D_E>34.9 cm) [2].

related risks, or did not provide correlations were excluded. Relevant articles referenced by the chosen articles were included. The number of reviewed articles was 25.

For IQ v BH metrics, the query used was: ((“comput*”[Title] AND “tomograph*”[Title]) OR “ct”[Title]) AND “abdom*”[Title] AND “image quality”[Title] AND (“water*equivalent diameter”[Title] OR “diameter”[Title] OR “size”[Title] OR “body”[Title] OR “BMI”[Title] OR “habit*”[Title] OR “obes*”[Title] OR “overweight”[Title]) AND ((humans[Filter]) AND (2010:2024[pdat])). The number of retrieved articles was 19, from which articles related either to paediatric patients, dual energy CT, or contrast agent reduction techniques were excluded. However, relevant articles referenced by the chosen articles were included. The number of reviewed articles was nine, of which seven also included RD metrics.

3. Results

The inventory is provided in Tables 2, 3 and 4 which respectively list BH, IQ, and RD metrics. Further details on the metrics in a given category are discussed in separate sub-sections.

3.1. Inventory of body habitus (BH) metrics

The waist-circumference (WC) to hip-circumference (HC) ratio (WHR) was as expected correlated to WC (cm), sagittal diameter (cm), body mass (kg) and subcutaneous and visceral fat area (cm^2) [16,18]. It was noted that antero-posterior (AP) and WC correlated better with amount of visceral and subcutaneous fat than WHR, in both men and women. Furthermore, since men and women have different amounts of visceral and subcutaneous fat, the slope of the regression of AP diameter to visceral fat was significantly different between genders [18] which suggests that any predications of dose or image quality metrics derived from WHR would be gender specific. Regarding ellipticity ratios, an initial set of reference values has been provided for various body regions both for adult and paediatric patients, where for the 297 abdomino-pelvic scans of adults (in the USA) included in the study, this ratio was found to be 1.48 [24].

Studies of Diagnostic Reference Levels (DRLs) based on D_E are well established [2,29]. The latter work categorised patients as small, average and large and based on $D_E \pm SD$, while the former, a more recent study, provided seven separate ranges based on T-shirt reference sizes for D_E as estimated from localiser radiographs. These ranges ran from XXS to XXL and were defined separately for each body region [2]. Recent work has shown that water equivalent diameter (D_w) varies minimally with tube potential, indicating that it is a robust metric of patient size [30] but does depend on an accurate delineation of the patient boundary [22,24,28,31–36]. D_w should be evaluated along the entire patient scanned volume [25], although works have evaluated the suitability of using a single central slice [37] or a subset of slices or even localiser radiographs [22,25,38,39], and showed it is still possible to achieve an accurate size specific dose estimate (SSDE). DRLs for neck, chest, abdomen and pelvis, stratified by D_w, have been determined for the USA, where D_W was evaluated at a single slice at the centre of the imaged region [40].

3.2. Inventory of image quality (IQ) metrics

While there are many IQ metrics [59], this work focused only on objective metrics derived from patient images which are related directly to sharpness, contrast, noise magnitude/texture and perceived detectability. Global measurements such as global noise level (GNL) enable a practical approach to ensure protocol consistency over time and to also define broad thresholds for acceptable noise levels in images [60]. Regional measurements are more relevant for individual protocol optimisation based on particular clinical queries and pathologies. Moghadam et al evaluated abdomino-pelvic image noise by placing a 1000 mm^2 region of interest (ROI) in the liver [29]. For contrast-to-noise ratio (CNR) measurements in the abdomino-pelvic region, the contrast was determined by drawing ROIs in various organs and regions: liver [61] – with some studies using liver segments II, VII [13] or right lobe [62]; paraspinal [62] or psoas muscles [54]; spleen [13]; arteries [13,62]; subcutaneous fat [13,62]. ROI dimensions were in the range 100–200 mm^2. Some works investigated the use of CNR to assess image quality in iterative reconstruction [61,62], although it has been noted that CNR has limited applicability in iteratively reconstructed images due to the non-linear nature of the process (further discussed below) [59,63]. One study used margin sharpness (MS) in the evaluation of sharpness of borders between liver lesions (cysts, metastasis, haemangiomas, abscesses, fat deposition, lacerations, focal nodular hyperplasia, and hepatocellular carcinomas) and liver adjacent tissue [50]. Each lesion, together with the liver boundary, was segmented manually by trained radiologists. The authors noted that this metric is highly susceptible to confounding factors such as the use of contrast agents or physical parameters such as tube voltage or slice thickness. Similar to MS, structure sharpness index (SSI) was evaluated as the gradient across a feature-to-adjacent tissue interface, in particular in relation to vessel sharpness in contrast enhanced CT [57].

The system response function (also known as transfer function) of modern CT scanners is neither linear nor shift invariant. In addition, noise is not wide-sense stationary. Very importantly, in the case of modern iterative reconstruction techniques, a final regularisation step based on *a priori* knowledge of abdomino-pelvic images is also included in the image reconstruction. In view of this, values of sharpness (such as MTF) and noise texture (such as NPS) measured on test-objects will not transfer unmodified to the reconstructed image but become a function of the local contrast and noise in the ROI in the patient image [64–68]. Hence in the case of studies of image quality directly from patient images any use of these metrics for the evaluation of image quality should be done *locally in the task-based region of interest (*e.g. *the task transfer function (TTF))*. An important quality metric found in the literature is the detectability index d'_{ind} [58]. This metric assesses the probability of detection of a predefined lesion were it to have been present in the patient and is based on the local task based MTF and NPS.

3.3. Inventory of risk/dose (RD) metrics

The dose length product (DLP) is readily available on CT systems but based on a standard 32 cm cylinder and hence not a true measure of the energy imparted to the individual patient. The SSDE attempts to provide a better estimate of the latter.

Table 3
Image quality metrics for abdomino-pelvic CT optimisation.

Quality category	Image quality metric	Definition and unit	Measure/estimate of what?	Measurement method and instant of determination (all post scan since derived from patient images)	Use
Noise magnitude in an organ/tissue of interest.	Standard Deviation (SD).	SD (HU) of HU values over a manually placed homogenous ROI (2D or 3D). It should be noted that SD assumes spatially uncorrelated noise which is rarely the case in imaging systems, even more so in iterative reconstructed images. However we have not come across articles discussing the issue specifically in the case of CT imaging.	Variability of HU values across expectedly homogenous ROIs.	Manual placement of ROI. Value of SD is provided by the scanner software.	Traditional assessment of magnitude of image noise. Still used extensively [29] particularly for quick, on-the-fly assessment. An ROI placed in the surrounding air or the patient table can be used as a measure of noise produced by the scanner only, free from the influence of anatomical variability.
Noise magnitude across *whole* image.	Tian and Samei noise (TSN) [41].	Modal value in HU of the values of SD across areas of the *whole* image slice which do not include anatomical edges.	The most common value of stochastic noise across a *whole* image slice.	An image subtraction method is used to generate a noise map free of anatomical edges. Any remaining edges are then removed using an edge detection filter. SD values are divided by $\sqrt{2}$ to correct for image subtraction. The TSN is then the mode of all resulting SD values.	Objective and automated monitoring of noise as part of routine quality control and for comparing noise between different protocols and scanners. Interestingly, a regression analysis indicated that TSN *could be predicted* using the relationship: $TSN = B\sqrt{\exp(\mu D_w)}$, where B is a scanner, protocol and dose dependent parameter; μ is the attenuation coefficient of water at the effective energy level of the CT spectrum; D_w is the WED of the slice. This could in theory be used to adjust the protocol before scanning to produce a desired noise level.
Noise magnitude in *segmented* homogenous areas of interest in the image.	Global Noise Level (GNL) (the name is perhaps somewhat misleading given that it is actually applied to segmented tissue/organs) [42].	Modal value in HU of SD values of a noise map of an area of segmented homogenous tissue in a given slice (e.g. liver). Whilst TSN focuses on the whole image, the GNL invites us to focus on specific tissue types identified by simple thresholding. Specifically for their work, the authors focused on soft tissue areas of the image identified as pixels with a HU in the range 0:100HU. This could thus be used for the monitoring of noise levels in areas of the image *that would be most relevant to the clinical query* e.g., *liver*.	Gives the most frequent noise level in areas of homogenous tissue in a given CT slice.	A noise map is generated in which the value at each location corresponds to the SD in a 6 mm area (i.e., kernel) surrounding that pixel. A 'convolution method' was then used to calculate the SD for each kernel. The GNL is the mode of the SD values.	Suitable for automated monitoring of noise by measurements on predefined segmented areas of relative homogeneity in the abdomino-pelvic image slice relevant to the clinical query or several homogenous regions for a more global assessment. It is possible to use also homogeneous areas such as air and patient couch which are patient independent.
Noise structure.	Local Task-based autocovariance (ACV).	Task-Based Autocovariance (or Autocorrelation which is the autocovariance normalised to the value of autocovariance at (0, 0)): this refers to the autocovariance in the spatial domain of a sub-ROI in a uniform region of the task-based ROI [43].	Noise texture.	Measured post-scan. $\mathrm{nCOV}_i = \frac{1}{n-1}\sum_{\text{all } j \text{ in } S_i}\frac{\mathrm{COV}_{ij}}{\sigma_i \bullet \sigma_j}$, where i is the image pixel index at the central portion of images, j is a working image pixel index except i within a sub-region S_i, and σ_i and σ_j are the standard deviations at pixels i and j [44]. The values from ROI should b e detrended before calculation.	The shape, peak position and area under the ACV curve may be used to compare noise textures.
Noise structure.	Local task-based Noise Power Spectrum (NPS_{loc}) [45].	This refers to the NPS (again can be normalised as NNPS) of a sub-ROI in a uniform region of the task-based ROI. Under circumstances of wide-sense-stationarity the NPS is equal to the Fourier transform of the autocovariance (Wiener–Khinchin Theorem). In practice, small local ROIs are assumed to be wide-sense-stationary.	Noise texture.	Measured post-scan. $\mathrm{NPS}(u,v,w) = FT\{K(\tau_x,\tau_y,\tau_z)\}$, where τ is the distance between voxels, K is the autocovariance function and FT is the Fourier Transform [45].	The shape, peak position and area under the ACV curve may be used to compare noise textures.

(*continued on next page*)

Table 3 (*continued*)

Quality category	Image quality metric	Definition and unit	Measure/estimate of what?	Measurement method and instant of determination (all post scan since derived from patient images)	Use
Contrast between feature of interest and adjacent or surrounding tissue.	Contrast to noise ratio (CNR).	Mean difference in MPV in HU between the feature of interest (e.g. lesion) and MPV of adjacent tissue with respect to the value of the uncertainty in the difference. $\mathrm{CNR} = \frac{\mathrm{MPV}_{\mathrm{Subject}} - \mathrm{MPV}_{\mathrm{Background}}}{\left[SD_f^2 + SD_{bg}^2\right]^{1/2}}$. Several definitions of the CNR are found in the literature. We favour this definition as the uncertainty in the difference between the two quantities is the square root of the sum of the squares of the uncertainties. Moreover, in general the SD of feature and adjacent tissue are not equal so both must be considered. Again the presence of correlated noise would require modifications of the above expression for the CNR. Again we have not come across references discussing the issue specifically in the case of CT.	Measure of conspicuity of a feature with respect to the surrounding tissue.	ROIs are set up manually on homogenous regions of the feature and surrounding tissue and MPVs and their SDs read off directly.	The minimum value of the CNR for detectability is still a subject of research. Three levels of CNR may be defined: (a) The CNR level above which a detection can be considered a true-positive and a non-detection a true-negative at a given level of significance, (b) the minimum CNR level that may be expected a priori to lead to detection – can be used to set noise indexes at exposure such that lesions would be detected by the Radiologist or CAD software, (c) the CNR level beyond which a quantitative measurement of contrast can be performed with a stated uncertainty [46]. Some initial suggestions have been put forward ranging from 3 to 5 and which involve different definitions of CNR (e.g. [47–49]) but the authors feel that none appear to point to a firm conclusion if applied to CT.
Sharpness of feature-to-adjacent-tissue boundary.	Local Task-based line profile.	The smoothed sigmoid function describing the pixel values (in HU) along normals to the boundary between a feature and its adjacent tissue.	Organ/lesion boundary sharpness.	Graphical method obtained post-scan. A sigmoidal fitting function to the pixel values along the normal to the boundary may be obtained using [50]: $\underset{S,W,x_0,I_0}{\operatorname{argmin}} \sum_x \left[I(x) - I_0 - \frac{S}{1 + e^{-\frac{x - x_0}{W}}} \right]$, where x_0 is the position of intersection of the boundary and the normal to the boundary, x is the distance along the normal to the boundary, I_0 is the pixel value in HU at the point of intersection of the boundary to the normal, I is the pixel value in HU along the normal, S is the contrast (in HU) between the feature and adjacent tissue and W the distance (in pixels) over which the boundary occurs. Sanders et al [51] use a similar method to estimate the skin-air boundary sharpness. By representing the boundary as a polygon mesh and using each face of the mesh to set the normals.	
Sharpness of feature-to-adjacent-tissue boundary.	Local task-based Modulation Transfer Function (Task Transfer Function, TTF).	MTF derived from the Fourier Transform of the Line Spread Function derived from the Sharpness Line Profile.	Organ/lesion boundary sharpness. The TTF assess the spatial resolution under conditions of contrast and noise of the specific clinical task.	Graphical method obtained post-scan.	
Sharpness of feature-to adjacent-tissue boundary.	Margin Sharpness (MS) [50].	Gradient at the inflection point of the sigmoid function describing the pixel values (in HU) along the normal to the boundary between a feature and its adjacent tissue.	Measure of the sharpness for the boundary between a feature and the adjacent tissue.	The margin sharpness is defined as the gradient of the sigmoid fit: MS (HU) $= S/W$, where S is the contrast (in HU) between the feature and adjacent tissue and W is the distance (in pixels) over which the boundary occurs.	To quantify image sharpness across a boundary. The range of MS values for acceptable image quality is a subject of research and may be radiologist dependent.

(*continued on next page*)

Table 3 (*continued*)

Quality category	Image quality metric	Definition and unit	Measure/estimate of what?	Measurement method and instant of determination (all post scan since derived from patient images)	Use
Sharpness of feature-to-adjacent-tissue boundary.	Image Blur Metric (IBM) [52] implemented in MATLAB [53].	IBM is defined to range between 0 (minimum blur, maximum sharpness) and 1 (maximum blur, minimum sharpness).	Index quantifying degree of blur (or inversely sharpness) in an image.	Neighbouring pixel value differences in the image are compared with neighbouring pixel value differences in the same image after being subjected to a low pass filter. Large differences between the two images indicate low blur and are assigned low IBM values (i.e. high sharpness) in the original image and vice versa.	Can be applied to quantify the sharpness of a whole image [54] or specific ROIs [55].
Sharpness of feature-to-adjacent-tissue boundary.	Structure Sharpness Index (SSI) [56].	*Median* of the set of gradients ξ_l of HU profiles $\boldsymbol{I}_l$ along a set of equally but densely spaced (to eliminate placement bias) normal cross-boundary vectors $\boldsymbol{s}_l$ of equal length (s being the distance in mm along the normal) along the section of boundary of interest. In their implementation of the method, Chun *et al* prefer to use the *mean* [57], however Taubmann *et al* argue that the mean would be too susceptible to outlier gradient values corresponding to normals close to any random artefacts [56].	Measure of the sharpness of the boundary between a feature and the adjacent tissue.	The gradient of the slope of the least squares regression line fit is given by: $\xi_l = \frac{\mathrm{cov}[\boldsymbol{s}_l, \boldsymbol{I}_l]}{\mathrm{var}[\boldsymbol{s}_l]} = \frac{\sum_i \left(s_{l,i} - \frac{1}{N_l}\sum_j s_{l,j}\right)\left(I_{l,i} - \frac{1}{N_l}\sum_j I_{l,j}\right)}{\sum_i \left(s_{l,i} - \frac{1}{N_l}\sum_j s_{l,j}\right)^2}$, where s contains the distances in physical units of the N sample locations within the region of interest and I the corresponding intensities along profile line l. Taubmann *et al* and Chun *et al* have slightly different methods of choosing the range of s/HU values along the normal over which the regression is carried out.	To quantify image sharpness across a boundary. The range of SSI values for acceptable image quality is a subject of research and may be radiologist dependent. Taubmann *et al*'s method involves only one manual step which is to select the desired edge by roughly tracing it with a connected sequence of line segments. They then provide a MATLAB script for the rest of the process for objectivity. On the other hand, Chun *et al* provide a fully automated process.
Perceived detectability.	Detectability index d'_{ind} ('ind' as based on an individual patient scan).	A detectability metric based on the TTF and $\mathrm{NPS}_{\mathrm{loc}}$ that can in theory be measured on the patient image to provide an estimate of detectability of a predefined chosen lesion, e.g. a 10 mm circular lesion of a nominal HU contrast difference [58].		$d'_{\mathrm{ind}} = \frac{\left[\iint \lvert W(u,v)\rvert^2 \bullet \mathrm{TTF}^2(u,v)\mathrm{d}u\mathrm{d}v\right]^2}{\iint \lvert W(u,v)\rvert^2 \bullet \mathrm{TTF}^2(u,v) \bullet \mathrm{NPS}_{\mathrm{loc}}(u,v)\mathrm{d}u\mathrm{d}v}$, where $W(u,v)$ is the Fourier transform of the image of the chosen lesion in the spatial domain.	The use of the detectability index from patient images is not trivial and experience on clinical images is limited. However, work in this area is ongoing and it is hoped that tools for its evaluation in clinical practice would become more easily available to all in the near future.

Table 4
Risk/Dose metrics for abdomino-pelvic CT optimisation.

Risk/Dose metric and symbol	Definition and units	Measure/estimate of what?	Measurement method and instant of determination	Use
Dose Length Product (DLP)	$DLP(mGy.cm) = CTDI_{vol} \times L$ [69], where L is the length of the scan (cm) and $CTDI_{vol}(z)(mGy) = \frac{CTDI_w}{Pitch}$, [70]. $CTDI_w = \frac{1}{3}CTDI_{100,c} + \frac{2}{3}CTDI_{100,p}$ The $CTDI_w$ must be measured in a standard 32 or 16 cm PMMA phantom using the same exposure parameters (kV_p, mAs, bowtie filter, additional filter, pitch, collimation) used during the patient scan. The actual definition of DLP used may vary slightly including by scanner and whether tube current modulation is involved. A good discussion can be found in IAEA dosimetry code of practice [71] and appendix VII of the supplementary document on its implementation [72].	A measure of the total energy imparted to the standard phantom when exposed under the same exposure parameters as the patient. However it is important to note that DLP is not equal to the total energy deposited in the patient [73]. The nomenclature CTDIvol was introduced to differentiate it from CTDIw which was originally defined for axial CT; however, it should not be considered as implying that it is an average dose across the patient volume as its subscription might imply.	Measurements of $CTDI_w$ require the use of a pencil ionising chamber. Determined post scan since $\sum CTDI_{vol}(z)$ (or scan-length) or pre-scan since scan length is defined prior to scan. It can be read off from the DICOM dose report [74].	Since defined on a non-anthropomorphic phantom of fixed size, the DLP has little relevance to the actual energy imparted to the individual patient who varies in habitus/size [75]. Used mainly for DRL studies comparing doses for *similar protocols* between institutions [76–78]. Suitable also for comparison of relative doses for a fixed scanner from different protocols with *similar patient dose distributions* e.g. dose reduction from varying the exposure parameters for a given protocol or comparing alternative similar protocols [13].
Size Specific Dose Estimate (SSDE)	$\overline{SSDE}(mGy) = \frac{\sum_{z=1}^{N} SSDE(z)}{N}$, where $SSDE(z) = CTDI_{vol} \times cf$ is for a given slice and *cf* is a calibration factor which is a function of the Water Equivalent Diameter (WED) of the slice [23]. N is the total number of slices in the CT image.	Provides a better estimate of the total energy imparted to the patient by replacing the standard 32 cm PMMA phantom with a virtual disc water phantom having the same total attenuation as the patient slice [23].	Calculated post-scout or post-scan (latter being more accurate as it uses the measured values of linear attenuation of coefficient of patient voxels as inputs for the calculation of D_W). As of 2019, manufacturers are required to produce an SSDE value. [79].	Suitable for anthropomorphic phantom or patient optimization studies involving variable body habitus/size.
Individual organ dose (OD)	$D_T(mGy) = \frac{\bar{\varepsilon}_T}{m_T}$, where D_T is the mean absorbed organ dose, $\bar{\varepsilon}_T$ is the energy imparted to the tissue and m_T is the mass of the tissue [80].	Energy imparted per unit mass of an organ.	In the case of anthropomorphic phantoms, absorbed doses can be measured directly in different tissues/organs using TL, OSL or electronic dosimeters [81]. In the case of patients, voxel attenuation values would need to be converted to absorbed dose using MC based software involving modelling of the patient and imaging system [82]. Libraries of voxel models of patients of different habitus have been published and can be used to provide an approximate model for the individual patient. Other methods for absorbed dose calculation based on deep learning methods are being developed [83].	Necessary to subsequently evaluate organ risk or for estimates of effective dose.
Effective dose (full name 'organ dose based effective dose') (E or ED_{OD}).	$E(\text{or } ED_{OD})(mSv) = \sum_T w_T H_T$, where D_T are absorbed organ doses to a reference individual representing a given population and w_T are tissue weighting factors indicating organ/tissue radiosensitivity [84].	Measure of stochastic risk from an exposure to a reference individual representing a population [85]. However, there is only allowance for organ/tissue radiosensitivity and none for age and sex [86].	There are multiple approaches to the estimation of E [87]. May be estimated post scout or post scan depending on approach used.	Useful for comparing risks between different protocols *particularly when there are significant differences in absorbed dose distribution in the body* [88]. When time is limited, the Defining Organ Absorbed Dose (OD_D, mGy) defined as the "dose to an organ which is sensitive enough to be used as a primary radiation burden indication for a specific CT protocol and anatomical region" and thee corresponding effective dose ED_{OD} can be used. OD_D was defined as the absorbed dose to the stomach for the abdomino-pelvic exam [86].

(*continued on next page*)

Table 4 (*continued*)

Risk/Dose metric and symbol	Definition and units	Measure/estimate of what?	Measurement method and instant of determination	Use
Risk Index (RI)	$RI = \sum_T r_T OD_T$, where OD_T is the organ dose for organ T and r_T is a gender-, age-, and tissue specific risk of cancer incidence [86,89,90]. The units are number of cancers per 10^5 patients per 100 mGy.	This index is considered as the most reflective of the real patient risk and therefore *would be considered the gold standard* [86].	May be estimated post scout or post scan depending on approach used.	This would be the ideal metric to use.
Relative effective dose (ED_r)	$ED_r(mSv) = \frac{RI}{RI_{tp}} \times E$, where RI_{tp} is the RI for a 20 year patient [6,86,89].	The relative effective dose modifies the effective dose E to take into account age and sex specific factors.	May be calculated post scout or post scan depending on estimation approach used.	This metric was noted as having a very high linear correlation (r^2 of 0.99) with RI, the gold standard, which is expected given that EDr as defined is linearly related to RI [86]. This metric provides a modified dose measurement in mSv to take into account the ICRP's suggestion that effective dose may be adjusted by considering other risk factors.

In a paediatric abdomino-pelvic study comparing the difference between SSDE evaluated solely at a central slice and the actual mean SSDE evaluated along the entire z-axis of the patient as per definition, found at most an 11% difference, concluding that estimates from the central slice alone may provide a suitable substitute at least for paediatrics [35]. In other works, SSDE was also correlated with actual physical dosimetric measurements based on the CIRS© anthropomorphic phantoms [91,92] as well as Monte Carlo (MC) estimates along the *z*-direction on adult patients [93].

There are multiple approaches to calculate effective dose (E) described in the literature, and an effort to compare seventeen methods was carried out recently [87]. In this comparison, these methods were organised into three groups: (1) methods based on a lookup of the typical effective dose for the examination type as published in literature, (2) methods based on calculation from typical patient-specific values of CTDIvol and DLP multiplied by conversion factors, and (3) methods based on dose calculation software such as those provided by ImPACT, CT-Expo and the National Cancer Institute dosimetry system. The authors concluded that the value of E can vary by 6–18 times depending on patient size and method used, and recommend that the uncertainty associated with each method should be taken into account given the assumptions of patient age, gender and reference phantoms used. The results of such studies should therefore be approached with utmost care.

4. Discussion

The potential utility of a specific BH metric for the process of patient-specific protocol optimization and pre-scan choice of protocol depends on the strength of its correlation to IQ metrics relevant to the clinical task or to RD metrics (or both). Studies on correlations between RD and BH metrics and between IQ and BH metrics, are summarised in Tables 5 and 6 respectively. A discussion of the relevance of each set of correlation studies for protocol optimisation follows each respective table.

5. Correlation between Risk/Dose (RD) vs body habitus (BH) metrics

The retrieved articles that involved correlation of RD and BH metrics are provided in Table 5. The pertinent issues relevant to optimisation as elicited from the reviewed articles are discussed below:

System dependence: Correlations between RD and BH metrics are system dependent, because different manufacturers employ different approaches to current/voltage modulation and dose/noise reducing reconstruction algorithms. This has been highlighted both in purposely designed studies using phantoms [104] as well as patients [111,113], although these were not tested for statistical significance. In some studies, data from multiple systems was pooled, potentially masking these differences [29,33,78,98,106].

Use of modulation: In general, patient studies reported that RD metrics (commonly CTDIvol, DLP and SSDE) increased with increasing BH values (metrics commonly being BMI and D_W), irrespective of contrast agent use [40,98]. This indicates that whilst modulation approaches differ by manufacturer and model, they all to some degree attempt to maintain similar reference noise. However, whether this modulation was sufficient to retain clinically adequate image quality at large body sizes, has only been investigated in a very limited number of studies, which will be discussed in the following section. What can be concluded from the articles is that in the case of these specific studies going from the penultimate to the highest BH category did not lead to RD metric values tapering off, implying that modulation maximum current values were high enough to cater for the bigger patients; whether image quality was sufficient is of course another matter.

Effect of contrast agent: One study showing how RD increased with BH, stratified by contrast use, showed similar absolute dose values and dose increases irrespective of contrast use or otherwise [40]. This may be due to the inclusion of hundreds of facilities having a wide mixture of

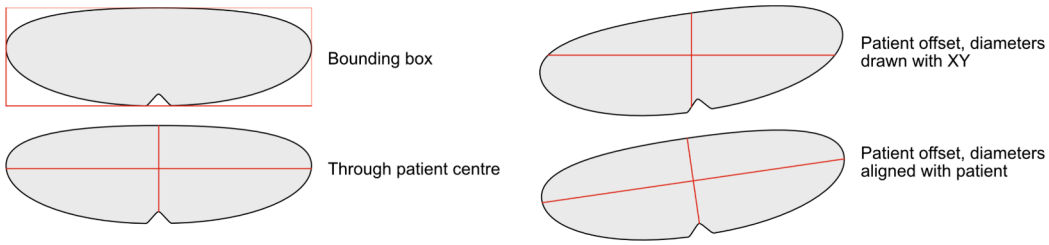

Fig. 1. Potential different approaches in determining the PA and LAT diameters. PA or LAT may be measured either as the maximum extent of the patient along the x and y axes (i.e. a bounding box) [22], or through the patient's centre whilst still being aligned along the x and y axes [28]. If the patient is rotated around the z-axes (i.e. not lying perfectly prone or supine), it may also be possible to measure the PA and LAT along the patient's axes.

scan protocols. Alternatively, Klosterkemper et al noted that contrast-enhanced (CE) studies had higher CTDIvol and SSDE for all patient size groups except the largest, in comparison with non-contrast-enhanced (NCE) studies [98]. Conversely, and for only average sized patients, Moghadam et al determined that contrast enhanced studies had CTDIvol, DLP, and SSDE lower than non-contrast enhanced studies, likely because whilst for a given sized patient the use of contrast increases D_W, it also permits the use of a lower mAs and hence CTDIvol when compared to a NCE study with a similarly sized patient [29,114]. Whilst both the latter studies had large sample sizes ($n > 500$) for each contrast group, this discrepancy was not tested for significance. A possible protocol-related reason that could explain lower doses for NCE studies in Klosterkemper et al's work is that the reference mAs was set in the range 120-150mAs for NCE, but 150mAs for CE. This discrepancy may also be explained by variability in the structure of multiphasic protocols, which was not discussed.

Correlation of RD to BH metrics: Five studies correlated RD with BH metrics [99,105], with three having small sample sizes [94,106,108]. The correlated RD metrics were DLP, SSDE and E, whilst the BH metrics were weight, BMI, AP+LAT, and adipose tissue volumes. Good correlation was found between CTDIvol and weight ($r^2 = 0.82$), and DLP and BMI ($r = 0.797$) [99], although DLP will vary with scan length. A limitation of these studies was that these correlations were not stratified by gender, potentially masking expected differences in fat quantity and distribution between male and female patients. Further, data was collected from only one scanner type (per study), so results may not necessarily generalise over various models, modulation and reconstruction algorithms. This distinction between male and female patients was noted by Funashima et al. (2023) [109], where although no correlations or tests for significance were performed, tabulated results indicated that absolute values of E for female patients were lower than for male patients in the three broad BMI categories investigated. Most of the studies reviewed did not explicitly set out to correlate RD with BH metrics. Indeed most were done for the purposes of establishing or reviewing DRLs in which stratification by BH metrics (most commonly BMI, D_W, or D_E) was included [2,29,40,98,110,111]. As such, although a general trend may be observed in these works, being that RD increases with each successive BH stratum, no correlations were reported. By the nature of DRL studies, pooling of examinations from multiple sites and systems, and pooling by gender, again, potentially masked system and patient specific correlations of RD with BH. Studies that explicitly target system and patient specific correlations with the large sample sizes typically associated with DRL investigations are thus needed.

Relating RD to BH metrics measured pre-scan: Studies that correlated or stratified RD according to BH used weight [94], BMI [96,99,101,105,108,109,111], D_W [27,40,98], D_E [29,78,110] or adipose tissue area/volume [99,105]. Weight or BMI are useful as they can be measured pre-scan, but have the limitation that they are global metrics which are not sensitive to tissue type or distribution. Metrics such as D_W and D_E may be evaluated as a function of longitudinal position along the patient, and in the case of D_W, it is also sensitive to tissue type and attenuating properties. The limitation of these metrics is that they are most accurately determined post-scan on the reconstructed axial images. However, there are approaches to estimate these metrics pre-scan. In the case of D_W, one option is the use of localizer radiographs [25]; in the case of D_E, an innovative approach was explored by Li et al (2022) [2] using T-shirt size.

Organ dose as an RD metric in correlation studies: Most of the reviewed studies investigating the relationship between RD and BH used CTDIvol, DLP and SSDE as the RD metrics [2,29,33,39,40,78,98]. A 2010 study investigating the correlation of patient weight with CTDIvol made use of the ImPACT dosimetry calculator, a set of pre-calculated MC tables, in order to derive individual organ doses [94]. These calculations were based on mathematical phantoms rather patients, limiting their suitability for patient-specific measurements. More accurate approaches exist today, notably ones which calculate organ doses via MC techniques and using actual voxel models based on patient images [83,115–117]. MC simulation has the added advantage that it is able to replicate mA modulation in 3D if such information is available [118]. Whilst there are a few articles investigating the use of MC to estimate organ dose, limited works applied MC to calculate organ dose as a function of body habitus [27,119]. A MC investigation by Fujii et al (2020) [27] noted increases in organ dose as patient size increased. While the system used tube current modulation (TCM), only one scanner was investigated and so could not investigate how the factor increase in dose changes across systems and manufacturers. Further, the sample size per BMI group was small ($n = 20$), with each sample being further split equally between male and female patients.

Desirable design features of future correlation studies: Future work is required that is specifically earmarked for investigating the correlation of RD with BH. Such work should ensure sufficiently large *patient* sample sizes from each stratum of BH, gender, CT scanner models, use or otherwise of modulation and type of reconstruction algorithm. The RD metrics should include organ doses derived using MC on voxel models based on actual patient images. This is complex because the MC simulation must model the individual scanner hardware. The BH metrics should, in addition to weight and BMI, as a minimum include D_E and D_W. If this research is conducted retrospectively, with RD and BH metrics estimated post-scan, the various relationships and correlations obtained may be useful to prospectively inform protocols that would be tailored for each gender and BH subgroup. Subsequently, pre-scan BH estimates may advise the selection of a suitable protocol which would reduce the need for re-scans and therefore avoid unnecessary dose.

6. Correlation between image quality (IQ) and body habitus (BH)

The nine reviewed articles that involved correlation between IQ and BH metrics are provided in Table 6. Seven articles of which included also RD metrics in addition to the IQ and BH metrics.

The pertinent issues relevant to optimisation as elicited from the reviewed articles are discussed below:

Phantom or patient based studies: Three studies were patient based [102,103,111], while four were phantom based [41,104,107,120]. Two

Table 5
Studies reporting correlation of RD with BH. Sample sizes are for abdomino-pelvic adult examinations only. TCM=Tube Current Modulation, CE=Contrast Enhanced, NCE=Non-Contrast Enhanced, FBP=Filtered Back Projection, IR=Iterative Reconstruction, CAP=Chest-Abdo-Pelvis, AP=Abdomino-pelvic. [A]Reconstruction algorithm (FBP/IR) not stated or not applicable. [B]Modulation includes any or all of: current, voltage, longitudinal, angular. [C]Studies not explicitly looking at the relationship between RDs and BHs. [D]Use of contrast medium not stated or not applicable. *Calculated by the authors from the published results.

Study (chronological)	Brief description	Results and comments	Note on IQ
Israel et al (2010) [94]	Patient based (n = 91, CE) study on one scanner[A] using modulation[B], compared CTDIvol and organ dose against patient weight (45.4–141.5 kg).	CTDIvol correlated with patient weight (r^2 = 0.82). From a 60 kg to a 100 kg patient, CTDIvol found to triple while individual organ doses noted to double.	No reference to IQ
Turner et al (2011) [95]	MC simulation phantom-based (six adult voxel phantoms) study on four simulated scanners[A] without modulation, investigated abdominal organ doses as a function of phantom circumference (66.5–124.5 cm).	As expected with fixed tube current, strong exponential decrease in abdominal organ doses with phantom circumference.	No reference to IQ
Chan et al (2012) [96]	Patient based (n = 100, CE) study on one scanner[A] using modulation[B], investigated the relationship of BMI (16.7–44.3 kg/m^2) on E, calculated as the DLP times a multiplicative factor *k*.	E was noted to increase with each successive BMI group, with values of 7.3, 8.9 and 12.0 mSv for low BMI (<20 kg/m2), normal BMI (20–25 kg/m^2), and high BMI (>25 kg/m^2) respectively.	No reference to IQ
Boos et al (2015) [97]	Patient based (n = 1942, CE and NCE) study[C] on one scanner with modulation[A], investigated CTDIvol, DLP stratified into five BMI groups.	Both CTDIvol and DLP increased with increasing BMI group, although no correlations were investigated.	No reference to IQ
Leng et al (2015) [33]	Patient based (n = 102)[D] study on four scanners[A] with modulation[B], compared two determinations of SSDE against D_W (20.6–42.7 cm).	SSDE determined from a single central slice agreed well with mean SSDE determined from a slice-by-slice approach over a wide range of body habitus.	No reference to IQ
Kanal et al (2017) [40]	Patient based (n = 249,502 NCE, n = 338,056 CE) multi-centre study[ABC] (n = 583), investigated CTDIvol, DLP, and SSDE as a function of binned D_W (21–41 cm).	CTDIvol, DLP, and SSDE increased by factors* of 2.9, 1.8, 3.3 in going from the smallest bin (21–25 cm) to the largest bin (37–41 cm), irrespective of contrast use.	No reference to IQ
Klosterkemper et al (2018) [98]	Patient based (n = 563 NCE, n = 1746 CE) study[C] on three scanners using modulation[B] and IR, investigated CTDIvol, DLP, and SSDE as a function of D_W bins as defined by Kanal et al (2017) [40].	Although overall lower than Kanal et al (2017) [40], CTDIvol and SSDE increased dramatically by factors* of 5.3 and 2.8 for CE, and 9.6 and 5.1 for NCE, from the smallest to the largest D_W bin size. A wider difference between NCE and CE was also noted.	No reference to IQ
McLoughlin et al (2018) [99]	Patient based (n = 239, CE) study on one scanner using modulation[B] and IR, investigated various tissue volumes against DLP for a range of BMI (13.9–49.1 kg/m^2).	DLP was found to be correlated significantly to BMI (r = 0.797).	No reference to IQ
Li et al (2018) [100]	MC simulation water-phantom-based study on one simulated scanners[A] without modulation, investigated dose to a water as a function of phantom diameter (6–55 cm).	Authors proposed a modified exponential relationship from that determined in other works [95].	No reference to IQ
Mehdipour et al (2019) [101]	Patient based (n = 73)[D] study[CA] (use of modulation not stated) investigated CTDIvol, DLP and SSDE stratified into seven weight bands. Patient weight and lateral diameters ranged from 38–105 kg and 23.7–46.4 cm.	CTDIvol, DLP and SSDE were noted to have increased by factors* of 3.9, 2.5, and 2 in going from the smallest weight band (38–50 kg, with a mean BMI of 18.6 kg/m^2 and mean LAT diameter of 27.9 cm) to the largest weight band (101–105 kg, with a mean BMI of 44.1 kg/m^2 and mean LAT diameter of 46.2 cm).	Investigation of Acceptable Quality Dose (AQD) where image quality was subjectively assessed by a radiologist.
Ria et al (2019) [102]	Patient based study[C] (n = 1061, CE) on two scanners with modulation[B], investigated the relationship between patient size (D_E=21.0–40.9 cm) and CTDIvol.	Median CTDIvol was noted to increase with each successive D_E reference range. From smallest to largest size group, this was 5 mGy (D_E=21.0–24.6 cm) to 16.7 mGy (D_E=37.0–40.9 cm), a factor of 3.34*.	Investigation of IQ noted in Table 6.
Ria et al (2020) [103]	Patient based study (n = 549, CE) on two scanners with modulation[B] and only IR, investigated the relationship between CTDIvol and D_W (20.3–42.1 cm).	CTDIvol increased with D_W for both scanners, as expected with modulation.	Investigation of IQ noted in Table 6.
Fujii et al (2020) [27]	Patient based (n = 80)[D] study[A] on one scanner using modulation[B], investigated MC derived organ doses as a function of D_W (21.8–30.5 cm), for the four BMI categories.	Liver, stomach and bladder, were noted to have a mean increase in organ dose of a factor* of 1.8 and 2.3 when going from normal to obese, and from underweight to obese, respectively.	No reference to IQ
Sookpeng (2020) [104]	Phantom based (in-house, physical) study on four scanners using modulation[B] and FBP, comparing CTDIvol between systems across a range of phantom diameters (19–30 cm).	TCM was noted to operate differently in different systems, with some having a wider margin of adjustment of tube current as the phantom size changes, and modulation may precede the phantom sections having a change in diameter (attenuation).	Investigation of IQ noted in Table 6.
Moghadam et al (2021) [29]	Patient based study[C] (n = 4,848 NCE, n = 14,541 CE) on eight scanners using modulation[B] and IR, investigated CTDIvol, DLP, and SSDE against D_E.	CTDIvol, DLP, and SSDE increased by factors* of 4.2, 3.9, and 2 in going from small (D_E<23 cm) to large (D_E>36 cm) patients. Pooled CE data showed lower CTDIvol, DLP, and SSDE compared to NCE.	Noise standard deviation was evaluated for 10 examinations per protocol, but not stratified by patient size.
Li et al (2022) [2]	Patient based study[C] (n = 500,580 CE and NCE) performed at 256 facilities[A], investigated CTDIvol, DLP, and SSDE against T-shirt size derived from D_E.	In going from XXS (D_E=18.2 cm) to XXL (D_E=39.6 cm): for NCE abdomino-pelvic exams, CTDIvol, DLP, and SSDE median values increased by factors* of 3.4, 3.5, and 1.5; while for CE abdomino-pelvic exams, CTDIvol, DLP, and SSDE increased by factors* of 3.5, 3.9, and 1.6.	No reference to IQ
Lee et al (2022) [105]	Patient based study (n = 695 CE) on scanners of the same model[A] using modulation[B], investigated effective dose E against BMI.	E was found to have a positive correlation with BMI (r = 0.715).	No reference to IQ
Hasan et al (2022) [78]	Patient based study[C] (n = 500 NCE, n = 528 CE) on five scanners using modulation[B] and IR, investigated CTDIvol and DLP between medium and large patients (D_E of	For abdominal pain (CE) CTDIvol and DLP both increased by a factor* of 1.5 in going from the medium size to the large size patient group.	No reference to IQ

(*continued on next page*)

Table 5 (*continued*)

Study (chronological)	Brief description	Results and comments	Note on IQ
	20–30, and 30.1–40 cm) and stratified over a number of clinical indications.		
El Mansouri et al (2022) [106]	Patient based study[C] (n = 30, CE) on two scanners[A] with modulation[B], compared SSDE as a function of AP+LAT size (43.06–64.25 cm).	Although SSDE was correlated with AP+LAT with r^2 = 0.69, the sample size was too small to provide statistical insight into how patient size affected CTDIvol and SSDE.	No reference to IQ
Tsalafoutas et al (2022) [107]	Phantom (Mercury 4.0, CTDI) based study on one scanner[A] with modulation[B], to evaluate the effect of said modulation and phantom size (D_W=16.5–35.2 cm) CTDIvol.	While CTDIvol was noted to generally increase with D_W, it was noted that the modulation curves were different depending on the direction of scanning and do not closely follow the D_W curve.	Investigation of IQ noted in Table 6.
Shah et al (2023) [108]	Patient based study (n = 61)[D] on one scanner using modulation[B] and FBP, investigated SSDE and E against BMI (13–26 kg/m^2).	D_W ranged between 18–33 cm. Correlations of SSDE with BMI and E with BMI were both weak with r = 0.54 and r = 0.39, respectively. Given the small sample collected from a single system, it is difficult to have any statistical insight.	No reference to IQ
Funashima et al (2023) [109]	Patient based study (n = 180)[D] on one scanner with modulation[B] and IR, compared effective dose E as a function of sex and BMI (lean, normal, obese): 18.5 < normal male < 28.1, 17.9 < normal female < 27.8 kg/m^2.	Although no correlations were performed, E for males and females both increased by a factor of 1.4 in going from lean to obese, with absolute values for females being slightly lower. This is perhaps the only work to provide BH and results stratified by gender.	No reference to IQ
Amalaraj et al (2023) [110]	Patient based study[C] (n = 363, NCE) on 14 scanners[A] with modulation[B], sought to establish DRLs for SSDE that are stratified by D_E.	Proposed SSDE NDRL values for the abdomen increased with D_E, from 11.2 mGy to 16.6 mGy for the 18–25 cm and 38–43 cm D_E groups, respectively.	No reference to IQ
Sebelego et al (2023) [111]	Patient based study[C] (n = 400)[D] on six scanners (5 with modulation[B] and using IR), reported CTDIvol, DLP and five SSDE methods stratified by BMI category.	For hospitals with results stratified by BMI category, all dose metrics were noted to increase with increasing BMI. It should be noted that one SSDE metric, obtained by applying a conversion factor to the BMI, would be expected to have such a relationship [112].	Investigation of IQ noted in Table 6.
Sebelego et al (2023) [113]	Patient based study (n = 403, CE) on two scanners with modulation[B] and IR, investigated the variation of SSDE and DLP with BMI.	For both systems independently, and with CAP and AP data pooled, both the SSDE and DLP increased with increasing BMI, although the SSDE in their case was evaluated as noted previously [111]. No correlations were evaluated for these.	Investigation of IQ noted in Table 6.

studies [107] made use of phantoms designed to assess TCM features (namely the Mercury© phantoms), whilst only one study [120] used anthropomorphic (CIRS©) phantoms to assess IQ. Although anthropomorphic phantoms may better represent heterogenous tissue within the patient, the mercury phantoms provide a wider range of patient diameters (up to 37 cm); the adult CIRS ATOM phantom is widest at the thorax with dimensions of 23x32cm [91]. Neither category of phantoms are suitable for the assessment of image quality for larger patient sizes. A further limitation of phantom based studies is that increased quantity of adipose tissue and its distribution in larger sized patients may affect the TCM in ways that may not be reproducible in a homogenous phantom [103]. Studies based on patients, evaluating GNL or noise standard deviation, noted that these IQ metrics were in general independent of BH (typically D_W) over multiple scanners, modulation and reconstruction algorithms. For these studies, D_W ranged from 20.3–42.1 cm, indicating a wide range of patient sizes. This may indicate either that the system TCM was sufficient to maintain a constant noise value, or more probably that non-linear IR approaches suppress noise even when the tube current would be insufficient [68]. The investigation of noise alone may not fully describe the IQ of the final image, and therefore it is important for future patient based studies to evaluate multiple IQ metrics as a function of BH.

Use of modulation: Tube-current modulation (TCM) seeks to provide consistent noise magnitude independent of patient size, however TCM may not always compensate sufficiently for larger patients [63,104,107]. One study investigated TCM across four scanners, and determined that for three systems (Philips, Siemens, Toshiba) using TCM, noise standard deviation increased with phantom diameter. The TCM current may max out and not properly adjust to a bariatric patient. Of course, the remedy to this is to increase the maximum allowable current. However, even that may not always be adequate. As noted by Szczykutowicz [63] the mA range alone is not sufficient to cater for a patient of any size, meaning that other parameters may need to also be modified in what the author refers to as 'size-based protocols': "Attenuation in CT increases exponentially with patient thickness. Indication to indication, dose changes by ~0.5 to 2 times. These dose changes are not changing exponentially with indication; dose changes as a function of patient size observed in diagnostic imaging are much larger than indication to indication dose changes […]. This means that to diagnose the same lesion in an infant as in a bariatric adult, the CT scanner must be capable of delivering doses ranging from sub mGy to about 100 mGy. This huge span in dose levels cannot be accomplished using a single kV, pitch, collimation, and rotation time. CT scanners do not have high enough mA limits to span this range in dose needs." One phantom-based study [107] investigating the effect of tube current modulation, noted that the detectability index d′ decreased with increasing D_W. This was in agreement with an earlier study [120] on an identical scanner which demonstrated that noise standard deviation increased when moving from a paediatric to an adult anthropomorphic phantom. However, the latter study also showed that a GE system did maintain the same noise standard deviation between phantom sizes. This emphasises that the effect of tube current modulation on IQ metrics is system dependent.

Limited range of image quality metrics used: Studies mostly evaluated noise, either as GNL or noise standard deviation in a particular organ. Although quite a few image quality metrics have been identified in literature (Table 3), most of these studies have not explored their dependence on BH. Whilst noise magnitude is an important IQ metric, other metrics, such as sharpness, contrast, and even noise texture (rather than only magnitude), need to be included to provide a complete description of the quality of the final presented image.

Limited range of CT systems studied: Most studies noted in Table 6 evaluated metrics on only one or two scanners. Correlations as well as any noise prediction models will be system dependent [103]. This limits the generalisability of these results, given the large number of combinations of scanner hardware and reconstruction approaches. Only the work by Sebelego et al. (2023) [111] evaluated IQ on six scanners, however this was only stratified by BMI, and no inter-system comparison was performed.

Table 6
Studies reporting correlation of IQ to BH. Sample sizes are for abdomino-pelvic adult examinations only. TCM=Tube Current Modulation, CE=Contrast Enhanced, NCE=Non-Contrast Enhanced, FBP=Filtered Back Projection, IR=Iterative Reconstruction, CAP=Chest-Abdo-Pelvis, AP=Abdomino-pelvic. [A]Reconstruction algorithm (FBP/IR) not stated or not applicable. [B]Modulation includes any or all of: current, voltage, longitudinal, angular. [C]Study for the purposes of establishing or evaluating DRLs. [D]Use of contrast medium not stated or not applicable. *Detectability index is not strictly included as part of the inventory in this work, but given the dearth of studies is included here for the purpose of highlighting the influence of TCM.

Study	Brief description	Results	Note on RD
Menke et al (2005) [39]	Phantom based study over a range of fixed tube current using FBP, to correlate noise standard deviation with increasing phantom diameter (D_W: 20–36 cm).	Expected exponential relationship for a linear FBP reconstructed images, at fixed tube currents between 50 and 250mAs.	Investigation of noise standard deviation as a function of D_W evaluated for a range of $CTDI_W$.
Solomon et al (2013) [120]	Anthropomorphic phantom (CIRS ATOM adult and paediatric) based study on two scanners (Siemens and GE) with modulation[B] and FBP/IR, investigated correlation between actual noise standard deviation with reference mAs for both FBP and IR.	For GE, noise was independent of phantom size, whilst for Siemens, noise standard deviation was higher for the adult phantom. For both systems, noise standard deviation was higher with FBP than with IR, with the difference being higher for the Siemens system.	No reference to RD
Tian et al (2015) [41]	Phantom (Mercury 2.0) based study evaluating noise standard deviation as a function of D_W (16–37 cm) on one scanner without modulation and using both FBP and IR, in order to derive a relationship to predict noise in patient images.	Relationship was dependent on D_W and reconstruction algorithm, as well as other CT hardware related parameters. This relationship was noted in Table 3 of this work as TSN.	No reference to RD
Ria et al (2019) [102]	Patient based study[C] (n = 1061, CE) on two scanners with modulation[B], investigated the relationship between patient size (D_E=21.0–40.9 cm) and GNL.	GNL was found to be only weakly correlated with patient size. One system (GE Discovery CT750HD) showed a slight decrease in noise with patient size, whilst a second scanner (Siemens SOMATOM Definition Flash) showed a slight increase in noise with patient size. These metrics were not correlated or tested for statistical significance.	Investigation of RD noted in Table 5.
Sookpeng (2020) [104]	Phantom based (in-house, physical) study on four scanners using modulation[B] and FBP, comparing noise standard deviation and CNR between systems across a range of phantom diameters (19–30 cm).	TCM was noted to operate differently in different systems, with some having a wider margin of adjustment of tube current as the phantom size changes. Only the GE scanner maintained similar noise SD across different phantom sizes.	Investigation of RD noted in Table 5.
Ria et al (2020) [103]	Patient based study (n = 549, CE) on two scanners with modulation[B] and only IR, investigated the relationship between D_W (20.3–42.1 cm) and GNL.	Findings were consistent with previous work on the same two systems [102]. Correlation and fitting parameters provided in terms of the proposed noise predictive models.	Investigation of RD noted in Table 5.
Tsalafoutas et al (2022) [107]	Phantom (Mercury 4.0, CTDI) based study on one scanner[A] with modulation[B], to evaluate the effect of said modulation and phantom size (D_W=16.5–35.2 cm) on detectability index* d′.	Detectability index d′ of five different materials decreased with D_W and was also noted to vary with phantom scan direction, even though CTDIvol was noted to increase with D_W.	Investigation of RD noted in Table 5.
Sebelego et al (2023) [111]	Patient based study (n = 400)[D] on six scanners with modulation[B] with FBP/IR, reported noise standard deviation stratified by BMI category (underweight, normal, overweight, and obese).	Authors noted that the noise standard deviation was independent of BMI category.	Investigation of RD noted in Table 5.
Sebelego et al (2023) [113]	Patient based study (n = 403, CE) on two scanners with modulation[B] and IR, investigated noise standard deviation with BMI.	Noise standard deviation was stratified for four BMI groups (underweight, normal, overweight and obese) and was noted to vary slightly with BMI, although no correlations were performed.	Investigation of RD noted in Table 5.

Effect of contrast agent: Most patient studies evaluating IQ in the abdomino-pelvic region involved the use of contrast agent, however, none investigated the effect of contrast use on IQ as a function of BH. One study [121] investigating the potential of reduced contrast use, did evaluate the CNR in routine CE (n = 46) and reduced CE (n = 46) over a range of patient weights (48.8–132.5 kg). The authors noted higher CNR in the routine CE, but did not correlate this with BH. The effect of contrast use on tube current modulation and the resultant effect on IQ metrics as a function of BH should be investigated.

Desirable design features of future correlation studies: Investigation of IQ metrics v BH should take into consideration a number of IQ metrics and not be limited to the use of noise standard deviation. Furthermore, such studies should be based on actual final reconstructed patient images. The study should look at a variety of CT scanner hardware, modulation systems and reconstruction algorithms, as these were noted to influence IQ. In terms of BH, sufficiently large patient samples are needed to ensure each patient size group is suitably represented. Separate correlations by gender are needed.

Seven studies considered correlations of IQ, RD, and BH metrics [39,102–104,107,111,113]. These studies show the emerging importance of considering BH related metrics in the evaluation of RD and IQ metrics. These studies were carried out for the purpose of evaluating or establishing DRLs, and as such a tabulation of RD and IQ metrics stratified by BH metric was sufficient. Future work should seek to investigate correlations between all three categories of metrics, and ideally include multiple metrics from each category, which should be technically manageable since many of them are measurable post-scan on the axial images. It would also be beneficial if the anatomical reference point where IQ and, in particular, the BH metric is measured, is noted. Studies involving multiple scanner hardware and modulation and reconstruction algorithm combinations would also be beneficial to highlight the manufacturer specific dependencies of these metrics.

7. Conclusion

In this review we emphasise that successful protocol optimisation in abdomino-pelvic CT must take into account three categories of metrics: Body Habitus/Size, Image Quality, and Risk/Dose. This is to our knowledge the first attempt to bring these three categories together in a comprehensive manner. We further emphasise that the BH category should be given increased importance, since it is critical for patient-specific pre-scan optimisation and protocol choice.

From this review 11 BH metrics, 12 IQ metrics, and 6 RD metrics were identified. Their definitions, methods used for measurement or calculation and their utility in practice were discussed.

It would seem that the current general consensus at present favours the use of D_W for BH, GNL for IQ and SSDE for RD. The limitation of D_W is that it is only precisely calculated post-scan, with localiser based approaches being only approximations. D_W further requires that the full patient anatomy be contained within the reconstructed field-of-view, a

condition which may not necessarily hold for larger sized patients. Since the SSDE is calculated via D_W, this would lead to an inaccurate dose calculation. SSDE does not provide organ-specific doses, making it ill-suited for higher-level optimisation studies. GNL is a noise metric, which, as noted earlier, may not be suitably sensitive to changes in CT tube current modulation.

It is suggested that future work should correlate a number of metrics from each of the RD and IQ categories with BH. The sample size should be large to ensure that each BH stratum, when further separated by gender, remains well represented. These correlations performed retrospectively and post-scan would be informative to understand which metrics are best suited for optimisation work. This would enable the creation of BH and gender specific protocols. It would also be beneficial to understand the correlation between BH metrics that may be measured prior to imaging, such as T-shirt size as proposed by Li et al [2], with more accurate BH metrics that are measurable post-scan, such as D_W, as this would inform on the appropriate protocol for the category of patient being imaged and clinical task prior to scanning.

The inter-relationship between IQ and RD as a function of BH is complex owing to patient-specific physical properties (e.g. quantity and distribution of adipose tissue) and is further compounded by the fact that modern systems employ various TCM modes, and by the non-linear nature of modern CT reconstruction algorithms. This makes it difficult to define metrics that are able to sufficiently predict the final image quality over a broad range of conditions.

In the case of BH metrics, D_w may be the most useful. This provides the combined attenuation contribution of various tissues at every axial slice, which is more informative than a global metric such as BMI or a regional metric that considers only patient geometry It may be determined accurately post-scan on axial images for the purpose of designing optimised protocols, and may be quickly estimated pre-scan (e.g. using scout images) to prospectively select the most appropriate optimal protocol. Multiple metrics are needed to fully characterise image quality, and if possible these should ideally be measurable in an automated fashion on the final reconstructed patient image [57]. Some metrics may be straightforward to implement and validate, such as the GNL [42]. Others, such as the SSI and noise texture and sharpness metrics, would be organ and task specific and whilst they may be useful for clinical query driven protocol optimisation, they might not be sufficient for imaging protocols where the radiologist would need to have good visual presentation of the entire patient as in the case of acute non-localised abdomino-pelvic pain. In the case of patient risk, the SSDE, being itself sensitive to patient tissue composition, may be easily implemented as a fast estimate of patient dose for day-to-day work. However since SSDE does not reflect individual organ doses, where deviations have been shown to be as high as 36% [119], this metric might be unsuitable for optimisation studies which include TCM. Instead, individual organ doses calculated via MC and voxelised patient image based models would be the gold standard approach [83]. The Risk Index as defined by BEIR VII, which sums the MC organ dose estimates, may then be calculated in order to report a single value of patient risk from the examination.

Finally, we propose a possible additional novel way forward. This inventory is intended to assist the clinical medical physicist in the optimisation of protocols. Such optimisation should ideally be targeted at addressing the image quality criteria for specific clinical tasks provided by internationally used guidance documents [122]. The metrics from the inventory should perhaps be mapped to the specific image quality criteria from these documents. As an example, a quality criterion for general abdomen CT in the aforementioned document is the visually sharp reproduction of the liver parenchyma and intrahepatic vessels. Under this proposal, images exhibiting acceptable 'visually sharp reproduction' as assessed by local radiologists would correspond to a specific range of values of the Structure Sharpness Index as determined by physicists. Using such an approach, radiologist-physicist teams can automate post-scan image quality checks in ways which would be acceptable to both.

Funding

This research did not receive any specific grant from funding agencies in the public, commercial, or not-for-profit sectors.

Declaration of competing interest

The authors declare that they have no known competing financial interests or personal relationships that could have appeared to influence the work reported in this paper.

References

[1] Brenner DJ, Hall EJ. Computed tomography — An increasing source of radiation exposure. N Engl J Med 2007;357. https://doi.org/10.1056/NEJMra072149.
[2] Li X, Steigerwalt D, Rehani MM. T-shirt size as a classification for body habitus in computed tomography (CT) and development of size-based dose reference levels for different indications. Eur J Radiol 2022;151:110289. https://doi.org/10.1016/j.ejrad.2022.110289.
[3] Scheirey CD, Fowler KJ, Therrien JA, Kim DH, Al-Refaie WB, Camacho MA, et al. ACR appropriateness criteria® acute nonlocalized abdominal pain. J Am Coll Radiol 2018;15:S217–31. https://doi.org/10.1016/j.jacr.2018.09.010.
[4] Hricak H, Brenner DJ, Adelstein SJ, Frush DP, Hall EJ, Howell RW, et al. Managing radiation use in medical imaging: a multifaceted challenge. Radiology 2011;258:889–905. https://doi.org/10.1148/radiol.10101157.
[5] Rehani MM, Nacouzi D. Higher patient doses through X-ray imaging procedures. Phys Med 2020;79:80–6. https://doi.org/10.1016/j.ejmp.2020.10.017.
[6] Samei E, Järvinen H, Kortesniemi M, Simantirakis G, Goh C, Wallace A, et al. Medical imaging dose optimisation from ground up: expert opinion of an international summit. J Radiol Prot 2018;38:967–89. https://doi.org/10.1088/1361-6498/aac575.
[7] Modica MJ, Kanal KM, Gunn ML. The obese emergency patient: imaging challenges and solutions. Radiographics 2011;31:811–23. https://doi.org/10.1148/rg.313105138.
[8] Rajapakse CS, Chang G. Impact of body habitus on radiologic interpretations. Acad Radiol 2014;21:1–2. https://doi.org/10.1016/j.acra.2013.10.006.
[9] Reynolds A. Obesity and medical imaging challenges. Radiol Technol 2011;82.
[10] Uppot RN. Technical challenges of imaging & image-guided interventions in obese patients. Br J Radiol 2018:20170931. https://doi.org/10.1259/bjr.20170931.
[11] Schindera ST, Nelson RC, Lee ER, DeLong DM, Ngyen G, Toncheva G, et al. Abdominal multislice CT for obese patients: effect on image quality and radiation dose in a phantom study. Acad Radiol 2007;14:486–94. https://doi.org/10.1016/j.acra.2007.01.030.
[12] Fursevich DM, LiMarzi GM, O'Dell MC, Hernandez MA, Sensakovic WF. Bariatric CT imaging: challenges and solutions. Radiographics 2016;36:1076–86. https://doi.org/10.1148/rg.2016150198.
[13] Bos D, Zensen S, Opitz M, Haubold J, Forsting M, Nassenstein K, et al. Image quality study of radiation-reduced combined chest and abdomen/pelvis CT compared with a standard protocol. Radiat Prot Dosimetry 2021;196:190–8. https://doi.org/10.1093/rpd/ncab147.
[14] Kataria B, Althén JN, Smedby Ö, Persson A, Sökjer H, Sandborg M. Assessment of image quality in abdominal CT: potential dose reduction with model-based iterative reconstruction. Eur Radiol 2018;28:2464–73. https://doi.org/10.1007/s00330-017-5113-4.
[15] Kalmar PI, Quehenberger F, Steiner J, Lutfi A, Bohlsen D, Talakic E, et al. The impact of iterative reconstruction on image quality and radiation dose in thoracic and abdominal CT. Eur J Radiol 2014;83:1416–20. https://doi.org/10.1016/j.ejrad.2014.05.017.
[16] Japan Society for the Study of Obesity. New Criteria for 'Obesity Disease' in Japan 2002;66.
[17] Lean MEJ, Han TS, Morrison CE. Waist circumference as a measure for indicating need for weight management. BMJ 1995;311:158–61. https://doi.org/10.1136/bmj.311.6998.158.
[18] Pouliot M-C, Després J-P, Lemieux S, Moorjani S, Bouchard C, Tremblay A, et al. Waist circumference and abdominal sagittal diameter: best simple anthropometric indexes of abdominal visceral adipose tissue accumulation and related cardiovascular risk in men and women. Am J Cardiol 1994;73:460–8. https://doi.org/10.1016/0002-9149(94)90676-9.
[19] Seung Wook S, Youn Seon C, Young Mee L, Do Kyoung Y, Kyung Hwan C, Myung Ho H, et al. The correlation between simple anthropometric indices and abdominal visceral fat accumulation by computed tomography. J Korean Acad Fam Med 2001.
[20] Storz C, Heber SD, Rospleszcz S, Machann J, Sellner S, Nikolaou K, et al. The role of visceral and subcutaneous adipose tissue measurements and their ratio by magnetic resonance imaging in subjects with prediabetes, diabetes and healthy controls from a general population without cardiovascular disease. Br J Radiol 2018:20170808. https://doi.org/10.1259/bjr.20170808.
[21] World Health Organization. Waist circumference and waist-hip ratio : report of a WHO expert consultation, Geneva, 8-11 December 2008 2011.

[22] Daudelin A, Medich D, Andrabi SY, Martel C. Comparison of methods to estimate water-equivalent diameter for calculation of patient dose. J Appl Clin Med Phys 2018;19:718–23. https://doi.org/10.1002/acm2.12383.

[23] Boone JM, Strauss KJ, Cody DD, McCollough CH, Toth TL. Size-Specific Dose Estimates (SSDE). Pediatric and Adult Body CT Examinations. American Association of Physicists in Medicine; 2011.

[24] Burton CS, Szczykutowicz TP. Evaluation of AAPM reports 204 and 220: Estimation of effective diameter, water-equivalent diameter, and ellipticity ratios for chest, abdomen, pelvis, and head CT scans. J Appl Clin Med Phys 2018;19:228–38. https://doi.org/10.1002/acm2.12223.

[25] McCollough CH, Bakalyar D, Bostani M, Brady S, Boedeker K, Boone JM, et al. Use of Water Equivalent Diameter for Calculating Patient Size and Size-Specific Dose Estimates (SSDE) in CT. American Association of Physicists in Medicine; 2014. https://doi.org/10.37206/146.

[26] Steiniger B, Klippel C, Teichgräber U, Reichenbach JR, Fiebich M. Can the size-specific dose estimate be derived from the body mass index? A feasibility study. Radiat Prot Dosimetry 2022;198:325–33. https://doi.org/10.1093/rpd/ncac038.

[27] Fujii K, Nomura K, Muramatsu Y, Goto T, Obara S, Ota H, et al. Correlation analysis of organ doses determined by Monte Carlo simulation with dose metrics for patients undergoing chest-abdomen-pelvis CT examinations. Phys Med 2020;77:1–9. https://doi.org/10.1016/j.ejmp.2020.07.016.

[28] Anam C, Mahdani FR, Dewi WK, Sutanto H, Triadyaksa P, Haryanto F, et al. An improved method for automated calculation of the water-equivalent diameter for estimating size-specific dose in CT. J Appl Clin Med Phys 2021;22:313–23. https://doi.org/10.1002/acm2.13367.

[29] Moghadam N, Lecomte R, Mercure S, Rehani MM, Nassiri MA. Simplified size adjusted dose reference levels for adult CT examinations: a regional study. Eur J Radiol 2021;142:109861. https://doi.org/10.1016/j.ejrad.2021.109861.

[30] McCollough CH, McCollough SL, Schneider JJ, Moen TR, Weaver JM, Vrieze TJ, et al. Dependence of water-equivalent diameter and size-specific dose estimates on CT tube potential. Radiology 2022;303:404–11. https://doi.org/10.1148/radiol.210860.

[31] Anam C, Haryanto F, Widita R, Arif I, Dougherty G. A fully automated calculation of size-specific dose estimates (SSDE) in thoracic and head CT examinations. J Phys Conf Ser 2016;694:012030. https://doi.org/10.1088/1742-6596/694/1/012030.

[32] Boos J, Kröpil P, Bethge OT, Aissa J, Schleich C, Sawicki LM, et al. Accuracy of size-specific dose estimate calculation from center slice in computed tomography. Radiat Prot Dosimetry 2018;178:8–19. https://doi.org/10.1093/rpd/ncx069.

[33] Leng S, Shiung M, Duan X, Yu L, Zhang Y, McCollough CH. Size-specific dose estimates for chest, abdominal, and pelvic CT: effect of intrapatient variability in water-equivalent diameter. Radiology 2015;276:184–90. https://doi.org/10.1148/radiol.15142160.

[34] MEDIRAD Project. Automatic Calculation of Water-Equivalent Diameter 2022. http://ctdose-iqurad.med.uoc.gr/autowed/(accessed April 24, 2022).

[35] Özsoykal I, Yurt A, Akgungor K. Size-specific dose estimates in chest, abdomen, and pelvis CT examinations of pediatric patients. Diagn Interv Radiol 2018;24:243–8. https://doi.org/10.5152/dir.2018.17450.

[36] Stratakis J, Myronakis M, Damilakis J. MEDIRAD. Implications of Medical Low Dose Radiation Exposure. Software tool (CT-IQURAD) module on radiation dose. 2021.

[37] Leng S, Shiung M, Duan X, Yu L, Zhang Y, McCollough CH. Size Specific Dose Estimation in Abdominal CT: Impact of Longitudinal Variations in Patient Size. 2013.

[38] Anam C, Haryanto F, Widita R, Arif I, Dougherty G. Automated calculation of water-equivalent diameter (D_W) based on AAPM task group 220. J Appl Clin Med Phys 2016;17:320–33. https://doi.org/10.1120/jacmp.v17i4.6171.

[39] Menke J. Comparison of different body size parameters for individual dose adaptation in body CT of adults. Radiology 2005;236:565–71. https://doi.org/10.1148/radiol.2362041327.

[40] Kanal KM, Butler PF, Sengupta D, Bhargavan-Chatfield M, Coombs LP, Morin RLUS. Diagnostic reference levels and achievable doses for 10 adult CT examinations. Radiology 2017;284:120–33. https://doi.org/10.1148/radiol.2017161911.

[41] Tian X, Samei E. Accurate assessment and prediction of noise in clinical CT images. Med Phys 2015;43:475–82. https://doi.org/10.1118/1.4938588.

[42] Christianson O, Winslow J, Frush DP, Samei E. Automated technique to measure noise in clinical CT examinations. Am J Roentgenol 2015;205:W93–9. https://doi.org/10.2214/AJR.14.13613.

[43] Smith TB, Abadi E, Sauer TJ, Fu W, Solomon J, Samei E. Development and validation of an automated methodology to assess perceptual in vivo noise texture in liver CT. J Med Imaging 2021;8. https://doi.org/10.1117/1.JMI.8.5.052113.

[44] Funama Y, Taguchi K, Utsunomiya D, Oda S, Katahira K, Tokuyasu S, et al. Image quality assessment of an iterative reconstruction algorithm applied to abdominal CT imaging. Phys Med 2014;30:527–34. https://doi.org/10.1016/j.ejmp.2014.02.005.

[45] Friedman SN, Fung GSK, Siewerdsen JH, Tsui BMW. A simple approach to measure computed tomography (CT) modulation transfer function (MTF) and noise-power spectrum (NPS) using the American college of radiology (ACR) accreditation phantom. Med Phys 2013;40:051907. https://doi.org/10.1118/1.4800795.

[46] Currie LA. Limits for qualitative detection and quantitative determination. Anal Chem 1968;40:586–93. https://doi.org/10.1021/ac60259a007.

[47] Bao Q, Chatziioannou AF. Estimation of the minimum detectable activity of preclinical PET imaging systems with an analytical method: minimum detectable activity estimation for preclinical PET. Med Phys 2010;37:6070–83. https://doi.org/10.1118/1.3495817.

[48] Hsieh J. Computed tomography: principles, design, artifacts, and recent advances. Second edition. Hoboken, N.J. : Bellingham, Wash: Wiley Interscience; SPIE Press; 2009.

[49] Rose A. Vision: human and electronic. New York: Plenum Press; 1973.

[50] Xu J, Napel S, Greenspan H, Beaulieu CF, Agrawal N, Rubin D. Quantifying the margin sharpness of lesions on radiological images for content-based image retrieval: Quantifying the margin sharpness of lesions. Med Phys 2012;39:5405–18. https://doi.org/10.1118/1.4739507.

[51] Sanders J, Hurwitz L, Samei E. Patient-specific quantification of image quality: an automated method for measuring spatial resolution in clinical CT images: an automated method for measuring spatial resolution in clinical CT images. Med Phys 2016;43:5330–8. https://doi.org/10.1118/1.4961984.

[52] Crete F, Dolmiere T, Ladret P, Nicolas M. The blur effect: perception and estimation with a new no-reference perceptual blur metric. In: Rogowitz BE, Pappas TN, Daly SJ, editors., San Jose, CA, USA: 2007, p. 64920I. https://doi.org/10.1117/12.702790.

[53] Bao DQ. Image Blur Metric. MATLAB Cent File Exch 2023. https://www.mathworks.com/matlabcentral/fileexchange/24676-image-blur-metric.

[54] Lee YJ, Hwang J-Y, Ryu H, Kim TU, Kim Y-W, Park JH, et al. Image quality and diagnostic accuracy of reduced-dose computed tomography enterography with model-based iterative reconstruction in Pediatric Crohn's disease patients. Sci Rep 2022;12:2147. https://doi.org/10.1038/s41598-022-06246-z.

[55] Park C, Choo KS, Jung Y, Jeong HS, Hwang J-Y, Yun MS. CT iterative vs deep learning reconstruction: comparison of noise and sharpness. Eur Radiol 2021;31:3156–64. https://doi.org/10.1007/s00330-020-07358-8.

[56] Taubmann O, Wetzl J, Lauritsch G, Maier A, Hornegger J. Sharp as a Tack: Measuring and Comparing Edge Sharpness in Motion-Compensated Medical Image Reconstruction. In: Handels H, Deserno TM, Meinzer H-P, Tolxdorff T, editors. Bildverarb. Für Med. 2015, Berlin, Heidelberg: Springer Berlin Heidelberg; 2015, p. 425–30. https://doi.org/10.1007/978-3-662-46224-9_73.

[57] Chun M, Choi JH, Kim S, Ahn C, Kim JH. Fully automated image quality evaluation on patient CT: multi-vendor and multi-reconstruction study. PLoS One 2022;17:e0271724.

[58] Smith TB, Solomon J, Samei E. Estimating detectability index in vivo: development and validation of an automated methodology. J Med Imaging 2017;5:1. https://doi.org/10.1117/1.JMI.5.3.031403.

[59] Verdun FR, Racine D, Ott JG, Tapiovaara MJ, Toroi P, Bochud FO, et al. Image quality in CT: from physical measurements to model observers. Phys Med 2015;31:823–43. https://doi.org/10.1016/j.ejmp.2015.08.007.

[60] Ria F, Wilson JM, Zhang Y, Samei E. Image noise and dose performance across a clinical population: patient size adaptation as a metric of CT performance. Med Phys 2017;44:2141–7. https://doi.org/10.1002/mp.12172.

[61] Baker ME, Dong F, Primak A, Obuchowski NA, Einstein D, Gandhi N, et al. Contrast-to-noise ratio and low-contrast object resolution on full- and low-dose MDCT: SAFIRE versus filtered back projection in a low-contrast object phantom and in the liver. Am J Roentgenol 2012;199:8–18. https://doi.org/10.2214/AJR.11.7421.

[62] Jensen CT, Telesmanich ME, Wagner-Bartak NA, Liu X, Rong J, Szklaruk J, et al. Evaluation of abdominal computed tomography image quality using a new version of vendor-specific model-based iterative reconstruction. J Comput Assist Tomogr 2017;41:67–74. https://doi.org/10.1097/RCT.0000000000000472.

[63] Szczykutowicz TP. The CT, handbook: optimizing protocols for today's feature-rich scanners. Medical Physics Publishing; 2020.

[64] National Electrical Manufacturers Association. Computed Tomography Image Quality (CTIQ): Low-Contrast Detectability (LCD) Assessment When Using Dose Reduction Technology 2017.

[65] Samei E, Bakalyar D, Boedeker K, Brady S, Fan J, Leng S, et al. Performance Evaluation of Computed Tomography Systems. American Association of Physicists in Medicine (AAPM); 2019. https://doi.org/10.37206/186.

[66] Brunner CC, Abboud SF, Hoeschen C, Kyprianou IS. Signal detection and location-dependent noise in cone-beam computed tomography using the spatial definition of the Hotelling SNR. Med Phys 2012;39:3214–28. https://doi.org/10.1118/1.4718572.

[67] Pelc NJ. Recent and future directions in CT imaging. Ann Biomed Eng 2014;42:260–8. https://doi.org/10.1007/s10439-014-0974-z.

[68] Richard S, Husarik DB, Yadava G, Murphy SN, Samei E. Towards task-based assessment of CT performance: system and object MTF across different reconstruction algorithms: Towards task-based assessment of CT performance. Med Phys 2012;39:4115–22. https://doi.org/10.1118/1.4725171.

[69] International Commission on Radiation Units and Measurements. Radiation Dose and Image-Quality Assessment in Computed Tomography. ICRU Report 87. J ICRU 2012;12. https://doi.org/10.1093/jicru/ndt006.

[70] American Association of Physicists in Medicine. The Measurement, Reporting, and Management of Radiation Dose in CT. Report 96. 2008.

[71] Dosimetry in diagnostic radiology: an international code of practice. Vienna: International Atomic Energy Agency; 2007.

[72] International Atomic Energy Agency. Implementation of the international code of practice on dosimetry in diagnostic radiology (TRS 457): review of test results. Vienna: International Atomic Energy Agency; 2011.

[73] Dixon RL. The physics of CT dosimetry: CTDI and beyond. Boca Raton, FL: CRC Press, Taylor & Francis Group; 2019.

[74] International Electrotechnical Commission. Particular requirements for the basic safety and essential performance of X-ray equipment for computed tomography. Geneva, Switzerland: 2016.

[75] McCollough CH, Leng S, Yu L, Cody DD, Boone JM, McNitt-Gray MF. CT dose index and patient dose: they are *not* the same thing. Radiology 2011;259:311–6. https://doi.org/10.1148/radiol.11101800.

[76] Dimitroukas CP, Metaxas VI, Efthymiou FO, Kalogeropoulou CP, Zampakis PE, Panayiotakis GS. Patient dose audit in common CT examinations. Radiat Phys Chem 2022;192:109924. https://doi.org/10.1016/j.radphyschem.2021.109924.

[77] European Commission. European Study on Clinical Diagnostic Reference Levels for X-Ray Medical Imaging. EUCLID. European Commission (EC); 2021.

[78] Hasan N, Rizk C, Babikir E. National Diagnostic reference levels based on clinical indications and patient size for adults' computed tomography in the Kingdom of Bahrain. Radiat Phys Chem 2022;197:110147. https://doi.org/10.1016/j.radphyschem.2022.110147.

[79] International Electrotechnical Commission. Methods for calculating size specific dose estimates (SSDE) for computed tomography. 2019.

[80] International Atomic Energy Agency. Diagnostic Radiology Physics: A Handbook for Teachers and Students. 2014.

[81] Zhang D, Li X, Gao Y, Xu XG, Liu B. A method to acquire CT organ dose map using OSL dosimeters and ATOM anthropomorphic phantoms. Med Phys 2013;40:081918. https://doi.org/10.1118/1.4816299.

[82] Li X, Samei E, Segars WP, Sturgeon GM, Colsher JG, Toncheva G, et al. Patient-specific radiation dose and cancer risk estimation in CT: part I. Development and validation of a Monte Carlo program. Med Phys 2010;38:397–407. https://doi.org/10.1118/1.3515839.

[83] Maier J, Klein L, Eulig E, Sawall S, Kachelrieß M. Real-time estimation of patient-specific dose distributions for medical CT using the deep dose estimation. Med Phys 2022;49:2259–69. https://doi.org/10.1002/mp.15488.

[84] International Commission on Radiation Protection. 1990 Recommendations of the International Commission on Radiological Protection. 1990.

[85] Martin CJ, Harrison JD, Rehani MM. Effective dose from radiation exposure in medicine: Past, present, and future. Phys Med 2020;79:87–92. https://doi.org/10.1016/j.ejmp.2020.10.020.

[86] Ria F, Fu W, Hoye J, Segars WP, Kapadia AJ, Samei E. Comparison of 12 surrogates to characterize CT radiation risk across a clinical population. Eur Radiol 2021;31:7022–30. https://doi.org/10.1007/s00330-021-07753-9.

[87] Avramova-Cholakova S, Dyakov I, Yordanov H, O'Sullivan J. Comparison of Patient effective doses from multiple CT examinations based on different calculation methods. Phys Med 2022;99:73–84. https://doi.org/10.1016/j.ejmp.2022.05.014.

[88] Vano E, Frija G, Loose R, Paulo G, Efstathopoulos E, Granata C, et al. Dosimetric quantities and effective dose in medical imaging: a summary for medical doctors. Insights Imaging 2021;12:99. https://doi.org/10.1186/s13244-021-01041-2.

[89] BEIR VII. Health Risks from Exposure to Low Levels of Ionizing Radiation: BEIR VII Phase 2. Washington, D.C.: National Academies Press; 2006. https://doi.org/10.17226/11340.

[90] Samei E, Tian X, Paul Segars W, Frush DP. Radiation risk index for pediatric CT: a patient-derived metric. Pediatr Radiol 2017;47:1737–44. https://doi.org/10.1007/s00247-017-3973-z.

[91] CIRS Tissue Simulation and Phantom Technology. ATOM® Dosimetry Phantoms. Models 701-706 2011.

[92] Moore BM, Brady SL, Mirro AE, Kaufman RA. Size-specific dose estimate (SSDE) provides a simple method to calculate organ dose for pediatric CT examinations. Med Phys 2014;41:071917. https://doi.org/10.1118/1.4884227.

[93] Li X, Marschall TA, Yang K, Liu B. Technical note: advancing size-specific dose estimates in CT examinations: dose estimates at longitudinal positions of scans. Med Phys 2022;49:1303–11. https://doi.org/10.1002/mp.15402.

[94] Israel GM, Cicchiello L, Brink J, Huda W. Patient size and radiation exposure in thoracic, pelvic, and abdominal CT examinations performed with automatic exposure control. Am J Roentgenol 2010;195:1342–6. https://doi.org/10.2214/AJR.09.3331.

[95] Turner AC, Zhang D, Khatonabadi M, Zankl M, DeMarco JJ, Cagnon CH, et al. The feasibility of patient size-corrected, scanner-independent organ dose estimates for abdominal CT exams. Med Phys 2011;38:820–9. https://doi.org/10.1118/1.3533897.

[96] Chan VO, McDermott S, Buckley O, Allen S, Casey M, O'Laoide R, et al. The relationship of body mass index and abdominal fat on the radiation dose received during routine computed tomographic imaging of the abdomen and pelvis. Can Assoc Radiol J 2012;63:260–6. https://doi.org/10.1016/j.carj.2011.02.006.

[97] Boos J, Lanzman RS, Meineke A, Heusch P, Sawicki LM, Antoch G, et al. Dose monitoring using the DICOM structured report: assessment of the relationship between cumulative radiation exposure and BMI in abdominal CT. Clin Radiol 2015;70:176–82. https://doi.org/10.1016/j.crad.2014.11.002.

[98] Klosterkemper Y, Appel E, Thomas C, Bethge OT, Aissa J, Kröpil P, et al. Tailoring CT dose to patient size. Implementation of the updated 2017 ACR size-specific diagnostic reference levels. Acad Radiol 2018;25:1624–31. https://doi.org/10.1016/j.acra.2018.03.005.

[99] McLaughlin PD, Chawke L, Twomey M, Murphy KP, O'Neill SB, McWilliams SR, et al. Body composition determinants of radiation dose during abdominopelvic CT. Insights Imaging 2018;9:9–16. https://doi.org/10.1007/s13244-017-0577-y.

[100] Li X, Yang K, Liu B. Radiation dose dependence on subject size in abdominal computed tomography: Water phantom and patient model comparison. Med Phys 2018;45:2309–17. https://doi.org/10.1002/mp.12888.

[101] Mehdipour A, Parsi M, Khorram F-S. Patient dose survey based on size-specific dose estimate and acceptable quality dose in chest and abdomen/pelvis CT examinations. Radiat Prot Dosimetry 2019;185:176–82. https://doi.org/10.1093/rpd/ncy288.

[102] Ria F, Davis JT, Solomon JB, Wilson JM, Smith TB, Frush DP, et al. Expanding the concept of diagnostic reference levels to noise and dose reference levels in CT. Am J Roentgenol 2019;213:889–94. https://doi.org/10.2214/AJR.18.21030.

[103] Ria F, Solomon JB, Wilson JM, Samei E. Technical note: Validation of TG 233 phantom methodology to characterize noise and dose in patient CT data. Med Phys 2020;47:1633–9. https://doi.org/10.1002/mp.14089.

[104] Sookpeng S, Martin CJ, Krisanachinda A. Design and use of a phantom for testing and comparing the performance of computed tomography automatic tube current modulation systems. J Radiol Prot 2020;40:753–73. https://doi.org/10.1088/1361-6498/ab8a56.

[105] Lee S, Kim KW, Kwon H-J, Lee J, Koo K, Song G-W, et al. Relationship of body mass index and abdominal fat with radiation dose received during preoperative liver CT in potential living liver donors: a cross-sectional study. Quant Imaging Med Surg 2022;12:2206–12. https://doi.org/10.21037/qims-21-977.

[106] El Mansouri M, Choukri A, Semghouli S, Talbi M, Eddaoui K, Saga Z. Size-specific dose estimates for thoracic and abdominal computed tomography examinations at two Moroccan hospitals. J Digit Imaging 2022;35:1648–53. https://doi.org/10.1007/s10278-022-00657-0.

[107] Tsalafoutas IA, AlKhazzam S, AlNaemi H, Kharita MH. Evaluation of automatic tube current modulation of CT scanners using a dedicated and the CTDI dosimetry phantoms. J Appl Clin Med Phys 2022;23:e13620. https://doi.org/10.1002/acm2.13620.

[108] Shah MA, Ahmad M, Khalid S, Qaseem SMD, Siddiqui S, Talib S, et al. Multivariate analysis of effective dose and size-specific dose estimates for thorax and abdominal computed tomography. J Med Phys 2023;48.

[109] Funashima K, Abiko S, Sato K. Novel method for calculating the effective dose using size-specific dose estimates conversion factors in abdomen–pelvis computed tomography. Radiol Phys Technol 2023;16:506–15. https://doi.org/10.1007/s12194-023-00738-x.

[110] Amalaraj T, Jeyasugiththan J, Satharasinghe D, Pallewatte AS. Dose reference level based on size-specific dose estimate (SSDE) and feasibility of deriving effective body diameter using tube current and time product (mAs) for adult chest and abdomen computed tomography (CT) procedures. J Radiol Prot 2023;43:011505. https://doi.org/10.1088/1361-6498/acb1bf.

[111] Sebelego I-K, Acho S, van der Merwe B, Rae WID. Size based dependence of patient dose metrics, and image quality metrics for clinical indicator-based imaging protocols in abdominal CT procedures. Radiography 2023;29:961–74. https://doi.org/10.1016/j.radi.2023.07.011.

[112] O'Neill S, Kavanagh RG, Carey BW, Moore N, Maher M, O'Connor OJ. Using body mass index to estimate individualised patient radiation dose in abdominal computed tomography. Eur Radiol Exp 2018;2:38. https://doi.org/10.1186/s41747-018-0070-5.

[113] Sebelego I-K, Acho S, van der Merwe B, Rae WID. Factors influencing size-specific dose estimates of selected computed tomography protocols at two clinical practices in South Africa. Radiat Prot Dosimetry 2023:ncad059. https://doi.org/10.1093/rpd/ncad059.

[114] Perisinakis K, Tzedakis A, Spanakis K, Papadakis AE, Hatzidakis A, Damilakis J. The effect of iodine uptake on radiation dose absorbed by patient tissues in contrast enhanced CT imaging: Implications for CT dosimetry. Eur Radiol 2018;28:151–8. https://doi.org/10.1007/s00330-017-4970-1.

[115] Jansen JTM, Shrimpton PC. Development of Monte Carlo simulations to provide scanner-specific organ dose coefficients for contemporary CT. Phys Med Biol 2016;61:5356–77. https://doi.org/10.1088/0031-9155/61/14/5356.

[116] Chen W, Kolditz D, Beister M, Bohle R, Kalender WA. Fast on-site Monte Carlo tool for dose calculations in CT applications. Med Phys 2012;39:2985–96. https://doi.org/10.1118/1.4711748.

[117] Sharma S, Kapadia A, Fu W, Abadi E, Segars WP, Samei E. A real-time Monte Carlo tool for individualized dose estimations in clinical CT. Phys Med Biol 2019;64:215020. https://doi.org/10.1088/1361-6560/ab467f.

[118] Deak P, Van Straten M, Shrimpton PC, Zankl M, Kalender WA. Validation of a Monte Carlo tool for patient-specific dose simulations in multi-slice computed tomography. Eur Radiol 2008;18:759–72. https://doi.org/10.1007/s00330-007-0815-7.

[119] Hardy AJ, Bostani M, Kim GHJ, Cagnon CH, Zankl MA, McNitt-Gray M. Evaluating size-specific dose estimate (SSDE) as an estimate of organ doses from routine CT exams derived from Monte Carlo simulations. Med Phys 2021;48:6160–73. https://doi.org/10.1002/mp.15128.

[120] Solomon JB, Li X, Samei E. Relating noise to image quality indicators in CT examinations with tube current modulation. Am J Roentgenol 2013;200:592–600. https://doi.org/10.2214/AJR.12.8580.

[121] Iyer VR, Ehman EC, Khandelwal A, Wells ML, Lee YS, Weber NM, et al. Image quality in abdominal CT using an iodine contrast reduction algorithm employing patient size and weight and low kV CT technique. Acta Radiol 2020;61:1186–95. https://doi.org/10.1177/0284185119898655.

[122] European Commission. European Guidelines on Quality Criteria for Computed Tomography. EUR16262. 2000.